Examining pelagic carbonate-rich sediments as an archive for authigenic uranium and molybdenum isotopes using reductive cleaning and leaching experiments

Matthew O. Clarkson[a*], Kim Müsing[a], Morten B. Andersen[b], Derek Vance[a]

Affiliations

[a]*Institute of Geochemistry and Petrology, Department of Earth Sciences, ETH Zürich, Clausiusstrasse 25, 8092 Zürich, Switzerland*

[b]*School of Earth and Ocean Sciences, Cardiff University, Cardiff, UK*

**Corresponding author:*

Email: matthew.clarkson@erdw.ethz.ch

tel :+41 44 632 45 78

This manuscript is published in Chemical Geology, DOI: 10.1016/j.chemgeo.2019.119412

Abstract

Novel metal isotope systematics are increasingly used to understand environmental change in geological history. On a global scale, the isotopic budgets of these metals respond to a range of environmental processes, allowing them to trace complex changes in the global climate system and carbon cycle. In particular, uranium (U) and molybdenum (Mo) isotopes are useful tools for quantifying the global extent of oceanic anoxia and euxinia respectively. The oceanic signature of these metals is recorded in contemporaneous marine sediments. Whilst, traditionally, organic-rich anoxic 'black shales' have provided a useful archive of these metals, carbonate sediments are increasingly being used as a passive recorder of ocean chemistry. The majority of published U and Mo isotope studies come from shallow water platform environments. By contrast, pelagic carbonate sediments are an under-explored archive for these metals, yet are widely available for important periods of Earth history. Despite their advantages, carbonates are a complex archive, containing multiple 'contaminant' components such as Mn-oxides, organic matter and detrital minerals. Each of these phases can have different metal concentrations and isotopic signatures, giving the potential to distort or bias the true oceanic signature recorded by the carbonate. Reductive cleaning procedures and selective leaching protocols can be used to avoid these contaminant phases, and are tested here on modern and ancient samples to judge their efficacy in isolating a 'carbonate-bound fraction'. To this end, leaching experiments were performed using different concentration acetic acid, HCl and HNO_3, on reductively cleaned and uncleaned sample pairs. The data demonstrate that Mn-oxide coatings and exchangeable phases have a large impact on the Mo isotopic signature (δ^{98}Mo) of carbonates, even when weak leaching techniques are used to preferentially dissolve them. Furthermore, detrital sources of Mo are also easy to liberate with different leaching protocols, and exert a significant control on leachate isotopic composition. The leaching studies identify that the pelagic carbonate end-member has a relatively high δ^{98}Mo, but the precise relationship to seawater compositions remains unclear. For U, significant contributions from non-carbonate phases can clearly be identified in higher concentration leaching acids using U/Ca ratios. However, U isotopes (δ^{238}U) show no resolvable difference with different leaching procedures and are not affected by reductive cleaning. This result probably reflects (a) the low potential for leaching refractory residual detrital U phases (e.g., zircon) that

48 contain the majority of U in the sample and (b) the low U inventories of Mn oxides versus those of Mo. Instead,
49 leaching likely extracts U that is mineralogically bound in carbonates and authigenic clays, which share a
50 common isotopic signature. These new data suggest that U incorporation into pelagic carbonates may be
51 dominated by adsorption, and be offset from seawater by ~ -0.15 ‰, in a similar manner to that seen for clays.

1 - Introduction

Novel metal isotope systems are part of a rapidly growing geochemical toolbox for reconstructing past environmental change, including understanding the co-evolution of life and the planet and the dynamics of the carbon cycle during past episodes of climate change. Of these tools, uranium isotopes (parent ^{238}U and ^{235}U; commonly reported as $\delta^{238}U$) have become popular for identifying and quantifying global-scale changes in oceanic anoxia in deep time (e.g. Brennecka et al., 2011a; Clarkson et al., 2018; Dahl et al., 2014; Dahl et al., 2017; Lau et al., 2017; Lau et al., 2016; Tostevin et al., 2019; Zhang et al., 2018a; Zhang et al., 2018b; Zhang et al., 2018c; Zhang et al., 2018d). Molybdenum (Mo) isotope measurements on contemporary sediments ($^{98}Mo/^{95}Mo$, reported as $\delta^{98}Mo$) are also widely used to estimate the extent of oceanic euxinia (anoxic and sulphidic conditions) (e.g. Arnold et al., 2004; Barling et al., 2001; Dickson, 2017; Duan et al., 2010; Kendall et al., 2017; Kendall et al., 2011). The sedimentary archives for these metals include both anoxic 'black shales' and oxic carbonates. The latter are a particularly attractive resource as they are ubiquitous in the geological record, have less geographical bias, less initial geochemical control on primary isotopic signatures (e.g. Andersen et al., 2014), and often contain useful additional geochemical and palaeotological information. Extensive work on U has shown that biogenic and non-biogenic platform carbonates can record an isotopic signature close to seawater, but often with a small positive offset that has been attributed either to fractionation during initial calcification or early-diagenetic processes (Andersen et al., 2017; Chen et al., 2018b; Romaniello et al., 2013; Stirling et al., 2007; Tissot et al., 2018; Weyer et al., 2008). To date, $\delta^{238}U$ from modern pelagic carbonates sediments have not been reported, although ancient pelagic carbonates have been inferred to represent seawater (Clarkson et al., 2018). There have also been suggestions that seawater $\delta^{98}Mo$ can be recorded in carbonates (Romaniello et al., 2016; Thoby et al., 2019; Voegelin et al., 2010; Voegelin et al., 2009), but records of $\delta^{98}Mo$ to date have largely come from black shales deposited in inferred euxinic settings, where Mo drawdown is close to quantitative (Arnold et al., 2004; Barling et al., 2001; Dickson, 2017; Kendall et al., 2017). This study represents the first characterization of Mo and U isotopes in pelagic carbonate-

77 rich sediments and presents initial constraints on the utility of these sediment as an archive for reconstructing
78 ancient seawater compositions.

79 The use of these metal isotope proxies in carbonate sediments relies on the fundamental assumption
80 that the carbonate-bound metals dominate the mass balance of a sample leachate, meaning that the
81 carbonate phase can be successfully isolated from a bulk sediment and that contributions from non-carbonate
82 components are insignificant. The extraction of the carbonate-bound metals is, however, extremely
83 challenging, as the sediments contain a complex mix of non-carbonate components that contribute
84 significantly to the total metal budget of a sample. Such 'contaminants' include easily exchangeable metals,
85 as well as metals incorporated into clays, crystalline Fe and Mn oxides, residual organic matter and detrital
86 minerals. Each component has very different metal concentrations, often much higher than pure carbonates,
87 and are typically isotopically different from each other and from seawater. Indeed, Fe-Mn crusts are known
88 to be a globally significant sink for Mo, and to a lesser degree U (Dunk et al., 2002; Kendall et al., 2017; Morford
89 and Emerson, 1999), and are ubiquitous in oxic sediments. If these phases are extracted in appreciable
90 amounts during sample processing they could contribute significantly to bulk carbonate measurements, and
91 therefore have the potential to influence secular isotopic trends observed in sedimentary records. They could
92 bias absolute values, or completely overwhelm the carbonate-bound signature in a manner that obscures any
93 ancient secular variation in seawater.

94 To isolate a carbonate isotopic signature from sediments the majority of studies employ a dilute acid
95 leaching technique, with the aim of selectively digesting the carbonate and avoiding significant contributions
96 from contaminant phases. Alternatively, some studies use more concentrated acid leaches in an attempt to
97 quantitatively extract metals from all phases in bulk samples, and then correct for any detrital component to
98 reconstruct carbonate signatures (Voegelin et al., 2010; Voegelin et al., 2009). Whilst this approach can avoid
99 the potential of leaching induced isotope fractionation, it also involves a large uncertainty in the
100 characterization of non-carbonate phases. Others have demonstrated the importance of removing metal
101 oxide bound contaminant phases in carbonate sediments using reductive cleaning protocols, in order to
102 acquire seawater-like metal concentrations (e.g. Boyle and Keigwin, 1985; Burton and Vance, 2000; Martin

and Lea, 2002; Pena et al., 2005; Russell et al., 1994). Such techniques have been used for metal isotope studies (Clarkson et al., 2018; Tostevin et al., 2019), but could also potentially introduce artefacts in final measured isotopic values due to the redox-sensitive nature of the cleaning procedure.

Currently, these different approaches have not been fully tested – for their efficacy or for the fidelity of the final isotope values with respect to the desired carbonate end-member. There is also great disparity in the methods used across a range of metal isotope systems. For U this includes buffered and unbuffered acetic acid based leachates, 0.25M HCl, 0.5M HCl, 1M HCl, 1M HNO_3 and 3M HNO_3 (Bartlett et al., 2018; Brennecka et al., 2011a; Clarkson et al., 2018; Dahl et al., 2014; Dahl et al., 2017; Elrick et al., 2017; Jost et al., 2017; Lau et al., 2017; Lau et al., 2016; Romaniello et al., 2013; Tostevin et al., 2019; White et al., 2018; Zhang et al., 2018a; Zhang et al., 2018b; Zhang et al., 2018c; Zhang et al., 2018d). Molybdenum extraction from modern platform carbonates has also used 3M HNO_3 (Romaniello et al., 2016) and 6M HCl or concentrated HCl for ancient and modern carbonate samples (Eroglu et al., 2015; Thoby et al., 2019). Whilst buffered acetic acid leachates can be successful for isolating carbonate components (Tessier et al., 1979), even dilute HCl is known to attack reactive Fe phases, silicate minerals and clays (Hirst and Nicholls, 1958; Leventhal and Taylor, 1990; Raiswell et al., 1994). The impact of these phases on metal isotopes is poorly understood. In particular, Mo is known to be highly mobile even in very dilute acids (Siebert et al., 2003) and no leaching tests have been published for Mo in carbonates. For U, a number of studies have tested a range of different acid strengths and concentrations for leaching platform carbonate samples. These studies yield $\delta^{238}U$ via different approaches that are identical within uncertainty (Lau et al., 2016; Zhang et al., 2018b), although contamination of the carbonate signature is possible via U released from apatite when using dilute HCl (Dahl et al., 2017). Additionally, trends in $\delta^{238}U$ across the Permo-Triassic boundary show excellent replicability, despite the use of different digestion protocols, which argues against significant leaching-induced artefacts (Zhang et al., 2018b). Step-wise leaching experiments on modern and ancient samples have, however, identified variability in $\delta^{238}U$, which is attributed to heterogeneities across different carbonate phases (Tissot et al., 2018; Zhang et al., 2018b) and can be avoided through complete dissolution of the carbonate. These results are promising but require further systematic testing, in particular for pelagic calcite sediments where U concentrations are

two orders of magnitude lower than originally aragonitic platform carbonates (Dunk et al., 2002; Reeder et al., 2001; Russell et al., 1994).

The general aim of this study is to provide a detailed examination of the U and Mo budgets of pelagic carbonate samples. Specifically, this study tests the potential importance of contaminant phases versus the desired pure 'carbonate-bound' U and Mo isotopic signatures, to assess the ability of different leaching and reductive cleaning techniques to avoid or remove these contaminant phases. To this end, a range of leaching experiments were performed, based on current literature protocols, that represents an increasing gradient of acid strength and concentrations. These were undertaken on reductively cleaned and uncleaned sample pairs, where the differences in the pairs can identify the presence and importance of metal oxide phases. Together these tests help identify the primary source of the contaminant (detrital material or metal oxides) and the optimum leaching protocol when these contaminants are insignificant, whilst also identifying any disadvantages of partial leaching. The study focuses on the cleanest extraction of the carbonate-bound component, but recognises that this will inevitably include primary carbonate precipitates, syn-sedimentary cements and later stage diagenetic phases. The relationship of the carbonate-bound component to seawater is then discussed to ascertain the potential for pelagic sediments to act as an archive for Mo and U isotopes, and the implications for paleo-seawater reconstructions.

2 - Methods

2.1 - Samples

The focus of this study is two deep sea sediment samples that represent modern (Holocene) and ancient (mid-Cretaceous) counterparts in terms of depositional setting and sedimentary components. They are mixed carbonate and siliciclastic sediments where the primary carbonate phase is low-Mg calcite. This is important for U since calcite has concentrations up to two orders of magnitude lower than aragonite due to differences in the co-ordination changes required to substitute U into the carbonate lattice (Reeder et al., 2001), making calcite rich sediments much more sensitive to potential contamination. The Holocene sample (ODP758) is a homogenized pelagic carbonate from ODP site 758, Leg 121 (Core 001H, Sect 01W, Interval 9-

12cm), deposited on the Ninetyeast Ridge, south of the Bengal Fan in the Indian Ocean (Peirce and Weissel, 1989). The sample age is approximately 4.4 to 6.4 kyrs (Burton and Vance, 2000). At this site, Holocene sediments are composed of clay-rich foraminiferal nannofossil ooze (Peirce and Weissel, 1989) with 61% carbonate (this study), no dolomite and an average of 0.16% organic carbon (Littke et al., 1991). The presence of Mn-oxide coatings in this sample has previously been identified through a decrease in Mn/Ca of picked foraminifera after reductive cleaning (Burton & Vance 2000). These coatings have been attributed to the precipitation of diagenetically mobilised Mn^{2+} (Burton and Vance, 2000) which would also form diffuse precipitates within the sediment. Mn-carbonate cements and overgrowths also occur in this sample, as identified by the highly elevated Mn/Ca of bulk digests compared to individual foraminifera (Boyle, 1983; Burton and Vance, 2000). These Mn-oxide phases are generally ubiquitous in carbonate sediments deposited under an oxygenated water column, although their preservation in ancient samples depends on later diagenetic processes. Despite containing Mn-oxides and Mn-carbonate overgrowths, the sample does not represent the interval of highest [Mn], and so does not contain the maximum possible contribution of Mn-oxide coatings.

The ancient sample (GA183) is a mid-Cretaceous pelagic to hemi-pelagic limestone from the Ghongzha section in Tibet (Bomou et al., 2013; Li et al., 2017), composed of mixed terrigenous and carbonate deposits with around 70% carbonate (this study) and no dolomite. Detrital components primarily include quartz, feldspar, plagioclase, and phyllosilicates (Bomou et al., 2013; Li et al., 2017). The sample was originally 1-2 cm of rock, representing ~500 yrs of deposition, and had previously been powdered using a mechanical agate crusher (Bomou et al., 2013; Li et al., 2017). The Ghongzha section is thought to have been deposited under a generally oxygenated water column, as evidenced by the ubiquitous presence of bioturbation, low total organic carbon and low redox sensitive metal concentrations. However, this sample will have experienced burial and diagenesis. Bulk Mn/Sr ~0.4 (this study) indicates a low degree of recrystallization, typical for low-Mg calcite sediments.

2.2 - Cleaning and leaching protocols

181 Sample cleaning and leaching protocols were designed based on commonly used methods for a
182 number of metal isotope systems (see Table 1). Although not a fully comprehensive study of all techniques in
183 the literature, the experimental design serves to illustrate the importance of different variables. Specifically,
184 the tests aim to assess: i) the success of reductive cleaning for removing contaminant Mn-oxide phases; ii) the
185 ability of weak acids to selectively digest carbonate and avoid non-carbonate contaminants and; iii) any
186 disadvantages of different leaching approaches, such as isotopic artefacts. The different acid concentrations
187 are used to identify mixing relationships between different contaminant phases and presumed carbonate end-
188 members.

189 For each cleaning and leaching test, approximately 200 mg of homogenised sample powder was
190 weighed into acid cleaned centrifuge tubes. All samples were rinsed three times with 50 ml of >18.2MΩ
191 'MilliQ' H_2O. Reductive cleaning was undertaken, to remove Mn-oxides, using a solution of 1M hydrous
192 hydrazine (analytical grade, Fisher Scientific) + 0.25M ammonium citrate in 16M ammonium hydroxide (Romil
193 UpA) (Bian and Martin, 2010; Boyle and Keigwin, 1985). Original protocols for reductive cleaning used 0.125M
194 citrate, but it has been suggested that a higher concentration citrate of 0.25M is required to successfully
195 remove secondary U and reach asymptotic U/Ca ratios in picked foraminifera (Bian and Martin, 2010). This
196 cleaning method has previously been applied to carbonate sediments from Oceanic Anoxic Event (OAE) 2
197 (Clarkson et al., 2018) and the Late Ediacaran (Tostevin et al., 2019) for U isotope analysis. 10 ml of the
198 reductive solution was added to the pre-rinsed sample and the centrifuge tube loosely capped to allow for
199 degassing. The centrifuge tube was then heated in a water bath for 30 mins at 90°C and regularly shaken by
200 hand to ensure continued sample-solution contact. The centrifuge tubes were then topped up to 50 ml with
201 MilliQ and the supernatant discarded. The sample was rinsed and centrifuged a further three times with 50
202 ml of MilliQ water to remove all traces of the cleaning solution.

203 Some protocols also include steps to remove exchangeable phases associated with oxides and clays,
204 such as pre-treatment with $MgCl_2$ (pH 7) or higher pH 1M sodium acetate rinses (pH 8) (Tessier et al., 1979),
205 but these methods were not included here. Instead we consider the reductive cleaning to remove both
206 exchangeable metals and more crystalline Mn-oxides, as the citrate effectively mobilises and chelates

exchangeable metals, including U (Alam and Cheng, 2014). Other studies also remove clays by flotation using an ethanol rinse (e.g. Pichat et al., 2003). Again this was not applied here, and whilst a total of 6 x 50ml of MilliQ rinses on the cleaned samples will float off some clays prior to leaching, a significant amount of clay is expected to still be present in the samples.

Separate leachates were performed on cleaned and uncleaned sample pairs. For acetic based solutions it is common to leach for between 6 and 48 hrs (Clarkson et al., 2018; Pichat et al., 2003; Tessier et al., 1979), with some studies (e.g. for zinc isotopes) also including heating to 60-70°C (John et al., 2017; Kunzmann et al., 2013; Pichat et al., 2003). For this study, 10 ml of the acetic based solutions was added to the sample and left to shake for 24hrs at room temperature. Two unbuffered acetic solutions (0.2M and 1M) were used to test the assumption that the leachate can self-buffer during digestion, as carbonate ion is released to solution, thereby preventing the dissolution of non-carbonate phases. For comparison, two buffered solutions were also used, namely 1M sodium acetate and 1M ammonium acetate, adjusted to pH 5. The buffered sodium acetate solution has been widely used for the preferential digestion of carbonate (after Tessier et al., 1979), but the high Na content creates problems for the chromatographic isolation of a pure metal fraction for isotope analysis. To avoid this, a high purity ammonium acetate buffer solution was tested as an alternative, and should have the same advantages of the sodium acetate solution in selectively digesting carbonate phases. The sodium acetate used was TraceSelect >99.999% (metal basis) (Fluka) and ammonium acetate was made from distilled acetic acid and ammonia solution, and pre-cleaned for trace metals through a Nobias PA-1 resin (Conway et al., 2013).

Hydrochloric and nitric acids were diluted from double-distilled concentrated solutions using MilliQ. Acid concentration was varied for the HCl based leachates from 0.2M to 7M as detailed in Table 1. Whilst these leachates include acids that are more concentrated than commonly used protocols, the evolution of different elements across this wider spectrum in acid concentrations allows better identification and tracking of the contaminant phases and mixing relationships. A 3M HNO_3 leachate was also included to compare to the 3M HCl, particularly to identify the potential impact of minor organic components in the sample. It should be noted, however, that both of the studied samples have very low TOC and this appears to have no significant

effect on metal budgets in these samples. For HCl or HNO_3 acid-based leachates, the acid is often 'added to completion', where the end of degassing signifies complete carbonate dissolution, or the sample is left in excess acid for 24 hrs (e.g. Zhang et al., 2018b; Zhang et al., 2018c). In this study, the acid volume was varied with acid strength in order to simulate the 'add to completion' approach. However, degassing was not immediately observed for the 0.2M and 0.5M HCl. The volumes were therefore scaled from 10 to 5 ml across the HCl leachates, as shown in Table 1, and the samples shaken for 1 hr. A longer leaching time period of 24 hours was also applied for selected HCl leachates, on cleaned and uncleaned sample pairs, to examine the impact of exposure time. Although volumes were not kept constant they do not represent a limitation of the study as they can still be used to investigate potential mixing relationships between contaminant phases. Additionally, the pH of the leachates was measured before and after digestion and reported in Table 1. All leachates were separated from the residues through centrifugation, and the supernatant pipetted into acid clean Savillex PFA beakers for chromatographic purification.

Total digests were performed on 60 mg bulk samples, and selected leachate residues were also treated in the same manner, using concentrated HF-HNO_3 at 140°C on a hotplate in Savillex PFA vials for 48 hrs. The digest was dried and treated with concentrated HCl, followed by Aqua-Regia to ensure the complete break-down of organic matter. The residue was then digested using concentrated HF-HNO_3 in a high pressure PAAR bomb at 210°C for 24hrs, in order to fully digest any residual refractory phases. The final residue was dissolved in 30ml 7N HNO_3 to ensure complete dissolution of any fluoride salts, before aliquoting for elemental concentration measurement.

253 ***2.3 - Trace and Major Element Concentrations***

254 Leachates and total digests were directly aliquoted and diluted 20 or 50 times in 2% HNO_3. Major and
255 trace elements were measured using a Thermo–Finnigan Element XR ICP–MS with an internal indium (In)
256 standard and a blank correction applied. Concentrations were calculated relative to an in-house, well
257 characterized and gravimetrically produced artificial standard with matrix characteristics similar to
258 carbonates. Isotope dilution was used to calculate U and Mo concentrations . All concentrations are reported
259 relative to the original uncleaned sample weight, as ppb (Mo and U), ppm (Mn, Sr, Al) or weight percent (wt.%;
260 Ca). Additionally, where metals are normalized to Ca these are reported as µmol/mol using the Element XR
261 data, except for Mo/Ca where ID-derived concentrations are used for Mo. Mn/Sr are presented as ppm/ppm,
262 as is the convention for carbonates. All data referred to in this paper (Al, Mn, Sr, Ca, Mo, U) are presented in
263 Tables 3 – 6. Additional concentrations that were measured on the Element XR (Li, Mg, Ti, V, Cr, Fe, Ni, Zn, Cd,
264 Ba, Ce), but do not feature in this paper, are reported in the Supplementary Material. Uncertainties on metal
265 concentrations and ratios are twice the relative standard deviation (RSD) of a carbonate standard which are
266 typically between 10 and 15%. In the case of U and Mo concentrations obtained by ID, uncertainties will be
267 much lower, at ≤1%.

268

269 ***2.4 - Carbonate measurements***

270 The percentage inorganic carbon for each sample was measured using a Coulomat and this was
271 converted to percent $CaCO_3$ by multiplying by 8.33. Although the samples do not contain dolomite they likely
272 also have minor Mn-carbonate phases, making the estimate of percent $CaCO_3$ an upper limit.

273

274 ***2.5 - Chromatographic separation and purification***

275 Sample leachates were aliquoted for Mo and U and spiked using a ^{97}Mo -^{100}Mo (Archer and Vance,
276 2008) and the IRMM-3636 U (Richter et al., 2008) double spikes. Chromatographic separation is modified from
277 the procedures of Bura-Nakic et al., (2018), using three column passes through the RE resin (Trisken
278 Technologies) and smaller load volumes in less concentrated HCl. Acetic based leachates were oxidized and

dried down with excess concentrated HNO_3, whilst HCl and HNO_3 leachates were simply dried down. The salt precipitates were then converted to chloride form with 7M HCl, dried and redissolved in 3ml 1M HCl ready to load on columns. Second and third column passes were loaded in 1ml 1M HCl. Prior to sample loading, ~0.2 ml 50-100μm RE resin was added to shrink-fit Teflon columns. Columns and resin were pre-cleaned with 2ml 0.2M HCl + 0.3M HF, rinsed with MilliQ water and pre-conditioned with 2 x 2ml 1M HCl. Matrix elements were eluted using 1M HCl, where the total rinse solution plus load solution equals 5ml. For the first and second pass, Mo and U were eluted together with 2ml 0.2M HCl followed by 2 ml 0.2M HCl + 0.3M HF but separated on the third column pass by the respective acids. Before analysis, samples were vigorously oxidized overnight with concentrated H_2O_2 and HNO_3 in order to break down minor resin contributions. Mo fractions were then re-dissolved in 0.2N HNO_3 and U fractions in 0.2M HCl for analysis. Total procedural blanks were ~120 pg for Mo and ~30 pg for U.

2.6 - Isotope measurements

Isotope ratios were measured on a Neptune Plus (Thermo– Finnigan) MC–ICPMS equipped with an Aridus II auto-sampler (CETAC) and using a PFA nebulizer and spray chamber (CPI) sample introduction system. Given the low concentrations in the leachates, 'standard + X-cones' were used for Mo and 'jet + X-cones' were used for U. Other instrument set up details are given in Archer and Vance (2008) for Mo isotopes and Andersen et al. (2015) for U isotopes.

Molybdenum isotope ratios are presented as:

$$\delta^{98}Mo = [(^{98}Mo/^{95}Mo_{sample}) / (^{98}Mo/^{95}Mo_{standard}) - 1] * 1000.$$

All Mo isotope compositions for samples are reported relative to NIST SRM 3134 = +0.25‰ (Nägler et al., 2014). For Mo, internal errors (2SE) for sample sizes >1ng were 0.01 – 0.1‰. Uncertainties are shown as ±2 standard deviations (2SD) for replicate measurements of the secondary standard NIST SRM-3414 (±0.1, n=24), except for the lowest intensity sample where the larger 2SE of ±0.2 is shown. Additionally, measurements were made of a modern ooid sample from Jolter's Cay, Bahamas, both with and without reductive cleaning

and leached in 1M sodium acetate, giving indistinguishable δ^{98}Mo of 1.98 ±0.02 (2SE), which is identical to published values from the same region (Voegelin et al., 2009). A blank correction (using the average procedural blank concentration of 120 pg) was applied to δ^{98}Mo, where the blank is assumed to be 0‰ in δ^{98}Mo. This correction has no significant effect, beyond analytical uncertainty, except for sample sizes of <1ng Mo where the blank is large enough to induce large corrections. For such samples the concentrations from isotope dilution are used, but δ^{98}Mo data are excluded.

Uranium isotope ratios are reported relative to the standard CRM-145 = 0‰ for $^{238}U/^{235}U$ and secular equilibrium for $^{234}U/^{238}U$, and presented as:

$$\delta^{238}U = [(^{238}U/^{235}U_{sample}) / (^{238}U/^{235}U_{CRM145}) - 1] * 1000$$

$$\delta^{234}U = [(^{234}U/^{238}U_{sample}) / (^{234}U/^{238}U_{sec.\ eq}) - 1] * 1000$$

Internal errors (2SE) for $\delta^{238}U$ measurements were typically 0.03 – 0.05‰, but up to 0.09‰ for very low intensity measurements (Tables 3-6). For U we use two secondary standards to assess external reproducibility and accuracy. First, a uraninite standard, CZ-1, used previously at ETH Zürich, was run between every five unknown samples and gives a $\delta^{238}U$ of -0.04 ±0.07‰ (n=66, 2SD) during the measurement period, which is identical to values reported elsewhere (Andersen et al., 2016; Andersen et al., 2015; Bura-Nakić et al., 2018; Stirling et al., 2007). Secondly, the modern ooid sample from the Bahamas was run repeatedly during the measurement period as a more closely matched secondary standard. There is no difference between cleaned and uncleaned leachates for this sample, which yield a $\delta^{238}U$ of -0.26 ±0.07‰ (n = 22, 2SD) that is in excellent agreement with values reported for other Bahamas ooid samples (Chen et al., 2018b; Romaniello et al., 2013). Self-bracketing CRM-145 also gives a $\delta^{238}U$ of 0.00 ±0.07‰ (n = 111, 2SD). Thus, uncertainties are shown as ±0.07‰, except for very low intensity samples where the larger internal error is shown.

2.7 - Cleaning Reagent Blank

It is not possible to purchase trace metal clean hydrous hydrazine, raising concerns of contaminant transfer from the reducing solution to the sample. It is assumed that the inclusion of citric acid acts as a chelating agent to bind the metals in solution, and prevents sample contamination. To test this assumption a homogenous synthetic $CaCO_3$ powder (99.999% calcite on trace metal basis; Acros Organics) was dissolved in duplicate in 10 ml of 1M sodium acetate solution, with and without reductive cleaning. From this exercise, a minor loss of Ca and Mn can clearly be seen in Table 2, which is a known phenomenon with reductive cleaning and caused by the partial dissolution of carbonate due to the presence of citric acid (Bian and Martin, 2010). This loss is associated with a minor decrease in U/Ca and no resolvable difference in Mo/Ca, suggesting that there is no significant addition of Mo or U blank to the sample.

3 - Results

3.1 - Ca, Mn and Sr

The modern sample ODP758 shows relatively uniform Ca concentrations across the range of acid strengths in both cleaned and uncleaned samples, and a constant decrease with cleaning (Fig. 1). The total digest liberated ~26 wt.% Ca, which is equivalent to maximum of 64 % $CaCO_3$ (assuming all Ca is carbonate bound), in close agreement with the Coulomat measurement (61% $CaCO_3$). The majority of the uncleaned leachates liberated 20 – 24 wt.% Ca, demonstrating that the leaching was largely successful at dissolving the carbonate (77 – 97% of total Ca). The exception is the 0.2M acetic and 0.2M HCl leachates, which dissolved 17 – 19 wt.% Ca (72 – 75% of total Ca). These lower Ca yields suggest that insufficient acid was available to ensure complete digestion of the carbonate, as also supported by the large pH changes during the experiment (Table 1). Cleaned leachates give consistently lower Ca yields (11 – 15 wt.%) than uncleaned leachates, reflecting the loss of almost half of the carbonate through reductive cleaning due to the presence of citric acid in the solution. Because of this loss of carbonate, the 0.2M acetic and 0.2M HCl leachates on cleaned samples were better able to ensure dissolution of the remaining carbonate fraction, producing yields comparable to the other acids.

352 Manganese shows relatively constant concentrations in all of the cleaned ODP758 samples (87 – 118
353 ppm; Fig. 1), despite different acid strengths. But the 24hr HCl leachates liberate ~50% more Mn (143 – 165
354 ppm). Similar concentrations are also seen for both cleaned and uncleaned samples treated with acetic acid
355 solutions and 0.2M HCl. By contrast, uncleaned ODP758 samples treated with more concentrated acids show
356 a dramatic increase, with Mn reaching up to 84% of total Mn (881 ppm) in the 7M HCl leach (626 ppm). These
357 differences are also generally reflected in Mn/Ca (Fig. 2), which identifies the source of Mn in the uncleaned
358 samples as Mn-oxides and highlights the success of reductive cleaning in removing Mn-oxide phases that
359 appear to be accessible primarily by the more concentrated leachate solutions. The increase in Mn in the
360 cleaned 24hr HCl leachates indicates some additional time dependent Mn contribution from silicate minerals,
361 but this is relatively minor compared to the Mn-oxide contributions removed with cleaning. The higher Mn/Ca
362 of the cleaned acetic and 0.2M HCl leachates (Fig. 2), relative to uncleaned samples, is likely due to the greater
363 relative loss of Ca from cleaning-related carbonate dissolution.
364 Similar trends in Ca yields are seen for GA183. The total digest contains 31 wt.% Ca, which is equivalent
365 to a maximum 77% $CaCO_3$, if all Ca is assumed to be carbonate bound, and comparable to the Coulomat
366 measurement (70%). Calcium yields from the majority of uncleaned leachates are between 88 and 98% of
367 total Ca (21 – 30 wt.%), except for the 0.2M acetic (69% of total) and 0.2M HCl (55% of total) leachates which
368 again show incomplete dissolution. All clean leachates have consistently lower Ca yields than the unclean
369 leachates, again demonstrating the partial dissolution of carbonate with reductive cleaning. In contrast to
370 ODP758, Mn in GA183 shows the same trends as Ca, with Mn yields close to that of the total digest. This results
371 in constant Mn/Ca for all leachates (Fig. 2), which indicates that the majority of the Mn is carbonate-bound
372 and that Mn-oxides are not present in the sample.
373 For GA183, the low Ca and Mn yields of 0.2M acetic and 0.2M HCl leachates (Fig. 1) is the result of the
374 leachate solution containing insufficient acid to fully digest the carbonate. This problem is worse in the
375 absence of cleaning due to the higher carbonate content of the sample. Both of these leachates also showed
376 large increases in pH during the experiment. The pH of the 0.2M acetic acid leachate was so high (pH 6) that
377 Fe-precipitates were observed to form in the supernatant after leaching. These were fully dissolved prior to

additional chemistry, after removal of the supernatant, with the addition of concentrated HNO_3, but if these phases started to precipitate during leaching they could impart additional isotopic fractionations for various metals.

Strontium generally follows the same trends as Ca in both samples, giving constant Sr/Ca for all leachates and indicating that Sr is primarily carbonate-bound, with no resolvable detrital source. Patterns in Mn/Sr (Fig. 2) are therefore related to differences in [Mn], and hence the leaching of Mn-oxides in ODP758. Cleaned samples of ODP758 show indistinguishable Mn/Sr, and both cleaned and uncleaned samples from GA183 show identical Mn/Sr for all leachates. The preservation of low Mn/Sr for GA183, similar to those for cleaned ODP758 samples, suggests a low degree of diagenetic recrystallization. However, it might also imply that the sample has experienced reducing conditions during early burial, which would have remobilised Mn and associated metals from Mn-oxides. It is also possible that the Mn-oxides were lost, but that any associated metals were transferred to carbonate phases or lost to the water column. The precise behaviour of trace metals in carbonates during diagenesis requires further investigation.

3.2 - Aluminium

Aluminium is generally assumed to be absent in pure carbonates, and therefore can be used to trace contributions from detrital aluminosilicate grains (Tribovillard et al., 2006). Aluminium yields are generally low in the 0.2M and buffered acetic acid leachates (ODP759: 32 – 138 ppm; GA183: 23 – 51 ppm), but a significant increase is seen in the unbuffered 1M acetic acid, HCl and HNO_3 leachates in both ODP758 (up to 2449 ppm) and GA183 (1410 ppm). Exposure time leads to an increase in Al, with concentrations reaching 4296 ppm in the unclean 24 hr 3M HCl leachate for ODP758, representing ~15% of total Al in the sample. The trends in Al clearly identify increasing detrital contributions in the more concentrated leachates, also reflected in Al/Ca. The increase in Al/Ca in the cleaned ODP758 samples relative to uncleaned samples (Fig. 2) is due to the loss of Ca through carbonate dissolution. The particularly low Al yields in the uncleaned 0.2M HCl leachates, relative to cleaned samples, are also seen in Al/Ca (Fig. 2), suggesting that some Al is being re-adsorbed onto the sample residue due to the low acidity of the solution. The re-adsorption effect would be more significant

404 in the uncleaned sample due to a higher total carbonate, and hence relatively lower available acidity. Notably,
405 the higher Al concentrations of the 1M acetic acid leachate compared to the buffered acetic solutions suggests
406 that, in this experimental set up, the dissolution of carbonate was unable to successfully buffer the acid,
407 leading to increased contributions from detrital sources even in this relatively dilute, weak acid.
408
409 ***3.3 - Uranium***
410 For ODP758, U yields show a general increase across the leaching acids from 66 – 94 ppb (U/Ca 0.061
411 – 0.087 µmol/mol) in the unclean acetic based leachates to 161 ppb in the unclean 7M HCl (U/Ca 0.139
412 µmol/mol) (Fig. 1 and 2). The highest U yield, from the 7M HCl leachate, is low compared to the total digest
413 (727 ppb, U/Ca 0.506 µmol/mol) indicating that at large proportion (~70-80%) of U is not leached from the
414 sample. For GA183, U shows only a minor increase from 52 – 61 ppb (U/Ca 0.35 – 0.045 µmol/mol) in the
415 acetic leachates up to 73 ppb (U/Ca 0.051 µmol/mol) in the 7M HCl leachate (Fig. 1 and 2). Similarly to ODP758,
416 the U yield from the 7M HCl leachate of GA183 is low compared to the total digest (463 ppb, U/Ca 0.259
417 µmol/mol) indicating that ~85% of total U is not leached by any of the acids (Fig. 1 and 2). For all leachates in
418 both ODP758 and GA183, U yields are consistently lower (54% and 31% respectively) in cleaned samples,
419 relative to the uncleaned samples (Fig. 1). In ODP758, the absolute U loss with cleaning is also reflected by a
420 minor but relatively constant decrease in U/Ca (0.02 – 0.03 µmol/mol) in the majority of the leachates, but
421 this is not seen in GA183 (Fig. 2, 3). Importantly, the decrease in U/Ca in ODP758 does not resemble the
422 behaviour of Mn (or Mo, see section 3.4) across the different leachate concentrations, suggesting that the U
423 loss is not primarily associated with a Mn-oxide pool but a result of carbonate dissolution during cleaning. For
424 ODP758, anomalously low U yields are identified in the uncleaned 0.2M HCl leach, and in both cleaned and
425 uncleaned 0.2M acetic acid and 0.2M HCl in GA183 (Fig. 1-3). Allowing the 0.2M HCl leach to continue for 24
426 hrs in did not improve U yields to a level comparable to other leachates. These low absolute U yields are also
427 reflected in low U/Ca for the unclean 0.2M HCl leachates in both samples, which could be indicative of both
428 incomplete carbonate digestion and the re-adsorption of U onto the residue.

For ODP758, U/Ca shows a positive linear correlation with Al/Ca, with both cleaned (R^2 = 0.91) and uncleaned (R^2 = 0.62) sample sets showing approximately parallel trends (Fig. 4). The 24hr HCl leachates tend to liberate more Al relative to U, plotting to the right of the best fit lines (Fig. 4). This suggests liberation of U associated with an alumino-silicate mineral phase as acid concentration increases, although clearly ODP758 has a much larger pool of silicate associated U.

Despite detrital U contributions being evident in U/Ca for ODP758 the $\delta^{238}U$ is invariant between the leachates, with an average of -0.50 (±0.06, 1SD) ‰ for uncleaned samples and -0.55 (±0.06, 1SD) ‰ for cleaned samples (Fig. 3). These are both lower than modern seawater (-0.39 ‰; Andersen et al., 2017). The residues from uncleaned samples and the total digest of ODP758 (n=3) have an average $\delta^{238}U$ of -0.35‰ (Fig. 4), which is indistinguishable from the detrital end-member previously identified for modern marine sediments at -0.32‰ (Andersen et al., 2016) and close to Bulk Silicate Earth (BSE) at -0.30‰ (Andersen et al., 2017). GA183 shows greater similarity between the leachates (-0.33 ±0.06 (1SD)) and the residues or total digests (average = -0.41‰) and there is no distinct $\delta^{238}U$ trend reflecting mixing of carbonate and detrital sourced U in the leachates (Fig. 4). Notably, two of the GA183 leachates (cleaned and uncleaned 0.2M HCl) appear anomalous, with higher $\delta^{238}U$ (-0.18 ± 0.07 ‰ and -0.23 ± 0.07 ‰) (Fig. 3) and the uncleaned sample has particularly low [U] relative to the majority of the leachates (Figs.1 – 4). In both the Holocene and ancient samples, these leachates demonstrate general features suggestive of incomplete dissolution and the potential re-adsorption of metals onto the residues, including low Ca, Mn, Al and U yields. Evidently, for U, this was significant enough in GA183 to introduce isotopic artefacts for the leachate. The unclean 0.2M acetic acid leachate does not exhibit anomalous $\delta^{238}U$, despite relatively low yields, suggesting that only the extremely poor U yields are problematic for this sample.

Data for $\delta^{234}U$ from leaching experiments are almost certainly dominated by artefacts due to the nature of the leaching process itself (Tables 3 – 6). For example, the leaching process will preferentially liberate ^{234}U from mineral lattice sites that have been damaged by decay, as in natural processes such as weathering (Andersen et al., 2009). Despite this, all of the leachates in ODP758 have $\delta^{234}U$ that are scattered around seawater (Tables 3 & 4), suggesting that they predominantly isolate carbonate phases (Andersen et al., 2010).

By contrast, the total digest is closer to secular equilibrium, indicating that silicate bound U dominates the isotopic budget of the sample, consistent with a $\delta^{238}U$ similar to BSE. This leaching artefact is also evident in GA183, where all leachates are highly enriched in ^{234}U. The corresponding depletions of ^{234}U that are caused by leaching can be seen in the residues.

3.4 - Molybdenum

Molybdenum concentrations in carbonates are extremely low, making analysis difficult. For this reason, analysis was only performed on ODP758. Cleaned acetic and 0.2M HCl leachates have consistently lower Mo concentrations (1.2 – 2.6 ppb; 0.004 – 0.008 µmol/mol Mo/Ca) compared to the uncleaned leachates (2.4 – 25.9 ppb; 0.005 – 0.056 µmol/mol Mo/Ca) (Fig. 5). Mo yields increase in the more concentrated acids, but the increase is more dramatic for uncleaned samples (up to 312 ppb; 0.61 µmol/mol Mo/Ca) than cleaned samples (up to 122 ppb; 0.47 µmol/mol Mo/Ca). The largest Mo/Ca difference between cleaned and uncleaned samples are for the 1 and 3M HCl leachates, suggesting that these two acids preferentially attack the Mn-oxide phases over silicate minerals. The 7M HCl leachates are more similar between cleaned and uncleaned samples, suggesting a greater dominance of silicate-derived Mo in these leachates. The Mo/Ca increase shows a positive correlation with Al/Ca in both cleaned and uncleaned samples (Fig. 6). For the cleaned samples the linear trend is clear, except for the 7M HCl which liberates significantly more Mo relative to Al than is the case for the other samples. The trajectory for the uncleaned samples is steeper than the cleaned samples, highlighting greater Mo liberation relative to Al in the more concentrated acids, and hence clearly identifying the liberation of Mo from Mn-oxides. Leaching for 24 hrs increases the Al yield relative to 1 hr, with relatively less additional Mo liberation, for both cleaned and uncleaned samples.

The trends described above for concentration data are consistent with the isotopic results. In particular, the impact of detrital components on Mo can also readily be identified for cleaned samples (Fig. 5 and 6), where the 0.5 to 7M HCl leachates fall on an apparent mixing line between the relatively high values of the 1M HCl leachate (2.11±0.1 ‰) and a silicate end-member (0.2 ‰) that is close to average upper continental crust (UCC) (0 ‰). The cleaned 0.5M HCl leachate shows greater silicate influences than the 1M

HCl (Fig. 6), with lower δ^{98}Mo and higher [Mo], despite being a more dilute leachate, suggesting that there is some heterogeneity of detrital material in the sample. Uncleaned samples generally show lower δ^{98}Mo than cleaned samples (Fig. 5), consistent with additional Mo contributions from a Mn-oxide-bound or exchangeable pool. The uncleaned 3M HCl leachate has a δ^{98}Mo most similar to modern Fe-Mn crusts and uncleaned sample residues, whilst greater silicate influence (closer to UCC) can be seen in the 7M HCl and 3M HNO_3 (Fig. 5). Figure 5 also shows that the uncleaned 1M acetic acid leachate has a distinctly lower δ^{98}Mo than the buffered leachates. In fact, it is more similar to 1M HCl, probably indicating the liberation of a Mo pool associated with Mn-oxides or detrital minerals.

4 - Discussion

4.1 - Efficacy of Reductive Cleaning

The cycling of Mo and U is strongly coupled to that of Mn in modern river, estuarine, continental slope and deep ocean environments, in both the water column and in sediments (Barnes and Cochran, 1993; McKee et al., 1987; Morford et al., 2009). Under an oxygenated water column, sediments become reducing at depth leading to the reduction of nitrate, Mn-oxides, Fe-oxyhydroxides and sulfate (Froelich et al., 1979). Upon reduction, manganese is released into porewaters and diffuses upward through the sediment to the depth of oxygen penetration, where it precipitates as Mn-oxides and Mn-carbonate. The Holocene sample studied here shows clear evidence for the presence of these Mn-oxides, in the difference in Mn/Ca ratios between reductively cleaned and uncleaned samples at higher acid concentrations, confirming previous inferences from Mn/Ca of picked and cleaned foraminifera (Burton and Vance, 2000). As stated in section 2.1, Mn-carbonate cements are also present in this sample, so that Mn/Ca found here for bulk samples are high compared to picked foraminifera (Burton and Vance, 2000). The ancient sample (GA183) does not show these differences across increasing acid concentrations (Fig. 1), implying that Mn-oxides are not present in this sample. If Mn-oxides had formed in this sample, in the oxic zone during sediment deposition, these could have

506 been lost through reduction during early burial diagenesis. The metals associated with Mn-oxide phases were
507 either lost to the water column or incorporated into Ca-Mn carbonate minerals.

508 Both U and Mo are sorbed to Mn-oxides in the oxic zone of the sediment as Mn-oxides precipitate
509 (Barling and Anbar, 2004; Kendall et al., 2017; Koschinsky and Halbach, 1995; Siebert et al., 2003; Wasylenki
510 et al., 2008) . Molybdenum can also be adsorbed to Mn-oxides as they form in and settle through the water
511 column (Kendall et al., 2017). For U, sorption results in an equilibrium isotope fractionation, where the
512 adsorbed species is ~0.2‰ lighter than the aqueous uranium (Brennecka et al., 2011b; Goto et al., 2014;
513 Jemison et al., 2016; Weyer et al., 2008). Molybdenum in natural Fe-Mn crusts has an isotopic composition ~
514 3‰ lighter than seawater (Siebert et al., 2003). The same Fe-Mn oxides as in crusts dominate the isotopic
515 mass balance of pelagic sediments, where Mo is adsorbed to diffuse Mn-oxide coatings (Siebert et al., 2003).

516 Molybdenum in the ODP758 leachates and total digest is clearly influenced by Mn-oxides. Mo/Ca
517 ratios in the ODP758 leachates are low for both cleaned and uncleaned samples, for acid strengths up to and
518 including 0.2M HCl (Fig. 5). For the 7M HCl leachate, both cleaned and uncleaned Mo/Ca ratios are very high.
519 For the 1M HCl and 3M HCl and 3M HNO_3 leachates, the values for uncleaned samples are high but those for
520 cleaned samples lower. This pattern, in combination with the available data for Mo isotope composition (Fig.
521 5), suggests that the 7M HCl leachates are impacted by both silicate-derived and Mn-oxide Mo, whereas in
522 more dilute acid leach solutions, the impact of reductive cleaning is clear – higher Mo/Ca in uncleaned
523 samples, lower δ^{98}Mo. A Mn-oxide end-member appears to be represented by the residue of the unclean 7M
524 HCl leachate, which gives a δ^{98}Mo of -0.6‰, close to Fe-Mn crusts (Siebert et al., 2003). This suggests that 7M
525 HCl has quantitatively leached the silicate fraction of Mo, but Mn-oxide bound Mo still remains in the residue.
526 Although Mn/Ca ratios are low in 0.2M and buffered acetic acid (Fig. 2), the higher Mo concentrations and low
527 δ^{98}Mo of uncleaned samples also suggest the presence of exchangeable Mo associated with Mn oxides that
528 are accessible to leaching. This occurs despite the fact that the Mn-oxides are not likely to be attacked by
529 these acids. This pool is liberated in all acids if reductive cleaning is not undertaken, with the result that
530 uncleaned leachates show generally low δ^{98}Mo.

By contrast, clear Mn-oxide influences are not seen in the U concentrations for ODP758, suggesting that the Mn-oxide associated U pool is insignificant for the mass balance of the sample. These differences are consistent with expected U and Mo contributions from Mn-oxide phases. Approximately 200 ppb of Mo is removed from the sample by reductive cleaning before the 3M HCl leachate, which must primarily represent Mn-oxides rather than dissolved carbonate because of the low Mo concentrations in the purest carbonate phases extracted by the weaker leachates. If the Mo:U ratio of the Mn oxides in the sample is the same as modern hydrogenetic Fe-Mn crusts (200; Koschinsky and Hein, 2003), only ~ 1 ppb of total sample U should be associated with the Mn-oxides, and removed with cleaning. This is insignificant for the isotopic mass balance of this sample, although it is also worth recognising that the presumed Mn-oxide end-member is also isotopically similar to the rest of the leachates (Fig. 4). Reductive cleaning of sample ODP758 does reduce U/Ca ratios significantly (Fig. 2, 4), and rather uniformly across all leachate solutions. It is clear that reductive cleaning leads to substantial dissolution of carbonate itself (Fig. 1), and it seems likely that the uniform reduction in U/Ca across all leach solutions could be due to heterogeneity in U/Ca, and preferential dissolution during reductive cleaning of a component with high U/Ca. Such differences are not seen for GA183, implying that the carbonate phase is more homogenous in terms of U concentrations, perhaps due to burial and diagenetic processes.

4.2 – Efficacy of selective leaching in isolating carbonate-bound trace metals

Increasing silicate associated contributions with increasing acid concentration were identified earlier for both Mo and U, but these non-carbonate contributions have quite different effects on the two isotope systems. Mixing of just two components explains Mo in the cleaned samples, where the carbonate-dominated leachate (with highest Ca/Mo; 1hr 1M HCl) has the highest δ^{98}Mo at 2.11 $\pm$0.10‰ and the non-carbonate end-member is consistent with a silicate contaminant that has a δ^{98}Mo (Ca/Mo = 0; δ^{98}Mo ~0.2‰) close to the composition of average UCC (0‰) (Fig. 6). Molybdenum release from detrital phases also appears to be time dependent, where the 24hr version of the cleaned 1M HCl leachate has a δ^{98}Mo closer to UCC at 1.00 $\pm$0.07‰ (Fig. 5). Although a seawater signature is not recorded in any of the cleaned carbonate leachates measured

here, the binary mixing trend identified suggests that a pure carbonate fraction would be isotopically relatively heavy and close to seawater. Further work is required to constrain the precise relationship. Whilst buffered acetic based leachates are often favoured for selective carbonate dissolution, 1M HCl appears to be the most effective here, but this must be dependent on the distribution of detrital minerals in the subsamples because the 0.5M HCl leachate shows greater detrital influences with a lower δ^{98}Mo (Fig. 6). A disadvantage of using acetic based leaching acids for δ^{98}Mo is that Mo is known to adsorb to clays in solutions at pH 2 – 7 (Goldberg et al., 1996) which would likely be associated with additional fractionation. This complexity is supported by the fact that the uncleaned 0.2M acetic acid, buffered acetic and 0.2M HCl (24hrs), with a final pH of 3.1 – 6, have relatively high δ^{98}Mo for their Ca/Mo, plotting close to the cleaned leachates mixing line in Fig. 6, consistent with a re-adsorption of isotopically light Mo.

In contrast to δ^{98}Mo, δ^{238}U does not display significant isotopic variation across different leachates, with an average of -0.55‰ for the entire ODP758 dataset and a variability ($\pm$0.10‰ (2SD)) comparable to that of the secondary standards ($\pm$0.07‰), making it difficult to clearly identify detrital influences in isotopic space. Whilst the residues are isotopically distinguishable at -0.35‰, the close similarity to the leachates would make it difficult to resolve any anticipated mixing relationship. This would certainly be the case for GA183, where the residues and leachates are almost indistinguishable. However, the generally low δ^{238}U of the ODP758 dataset, even in the 24 hr HCl leachates with lowest Ca/U (Fig. 4), is inconsistent with an extensive U contribution from a detrital phase that is characterized by the residues. Indeed, δ^{234}U in all ODP758 leachates are scattered around seawater (Tables 3 & 4), suggesting that they predominantly isolate authigenic phases (Andersen et al., 2010). Together, this suggests a lack of U leaching from the primary detrital U host in the sample, which represents >70% of U in the sample (section 3.3). This inference is consistent with the known occurrence of U in refractory minerals, including robust heavy minerals and accessory phases such as uraninite, zircon, apatite, coffinite and monazite. These minerals are either robust (e.g. zircon) or occur as inclusions within major silicate minerals such as biotite, amphibole or plagioclase (Ivanovich and Harmon; Pagel, 1982), and would be more difficult to leach. Moreover, the vast majority of accessible U in primary minerals is thought to be lost during terrestrial oxidative weathering and transport, generating depletions of

583 U relative to Th in pelagic sediments compared to the upper continental crust (Carpentier et al., 2013;
584 McLennan and Taylor, 1980; Tieh et al., 1980). This can be seen in both ODP758 and GA183, where Th/U of
585 the total digests (6.9 and 6.1 ppb/ppb) is elevated compared to bulk Earth (~3.8) (Blichert-Toft et al., 2010)
586 (Tables 3 & 5). Thus, the pre-depositional loss of accessible U may help prevent detrital U being leached from
587 detrital silicate minerals. The same mechanism could also be somewhat applicable to Mo, and therefore
588 explain why the 1M HCl leachate is not significantly influenced by detrital phases.

589 Rather than leaching of the primary detrital U host minerals, the positive correlation of U/Ca with
590 Al/Ca in ODP758, with no isotopic variation, is more consistent with the leaching of two distinct U pools that
591 have indistinguishable isotopic compositions but different mineralogical sources. We suggest that these two
592 different mineralogical components are i) carbonate-bound, and ii) clay-bound, and that both have a U
593 isotopic signature that is initially controlled by adsorption. Isotopic fractionation during adsorption to quartz,
594 clays and aquifer material has been demonstrated experimentally, with an offset of -0.13 $\pm$0.09 ‰ (1SD)
595 compared to dissolved U (Jemison et al., 2016). In a pelagic setting, as U is continuously supplied from the
596 overlying water column to porewaters it would adsorb to, and eventually be incorporated into, authigenic clay
597 minerals. This is predicted to create a clay-bound U pool with a $\delta^{238}U$ of ~ -0.55‰, which matches well with
598 the leachate data presented here (Fig. 3 and 4). Note that this cannot only be adsorbed U that remains as an
599 exchangeable phase, but it must eventually be stabilized into the mineral structure to generate the increase
600 in U/Ca with Al/Ca. The similarly low $\delta^{238}U$ of the acetic based leachates to the higher concentration acids
601 implies that U incorporation into the carbonate phase is also mediated by adsorption during syn-sedimentary
602 diagenesis, which has not been identified previously and is discussed in detail in section 4.3.

603 The above discussion assumes that ^{235}U and ^{238}U would be leached from the detrital phase with no
604 inherent preference. There have been suggestions that ^{235}U can be preferentially released from minerals
605 during leaching (Stirling et al., 2007). However, it is unclear if this is due to dissolution itself, or due to isotopic
606 heterogeneity in minerals (Stirling et al., 2007). Whilst it is possible that the more concentrated leachates have
607 selectively released ^{235}U from detrital phases, thereby masking the higher $\delta^{238}U$ signature of detrital U and
608 generating generally low $\delta^{238}U$ values, one might expect to see greater difference between the 1hr and 24hr

HCl leachates if significant dissolution driven fractionation were occurring. Furthermore, preferential leaching of the two isotopes is unlikely to explain the low $\delta^{238}U$ of the acetic based leachates.

4.3 - A common fractionation mechanism for authigenic U phases in pelagic sediments?

Uranium incorporation into carbonates is typically considered as a co-precipitation process (i.e. direct structural incorporation). Synthetic aragonite and calcite precipitation experiments suggest that there is no inherent isotopic fractionation during co-precipitation (Chen et al., 2016; Stirling et al., 2015), which also appears to be largely true for biogenic aragonite and calcite precipitation (Chen et al., 2018b; Romaniello et al., 2013; Stirling et al., 2007; Weyer et al., 2008). Small positive offsets (+0.12‰) have been observed in biogenic calcite and aragonite (Fig., 3, 5) and non-biogenic aragonite due to the specifics of aqueous U speciation (Chen et al., 2017; Chen et al., 2016). Chen et al., (2016, 2017) suggest that the charged species are preferentially incorporated into carbonate compared to the neutral uranyl species [$Ca_2UO_2(CO_3)_{3\ (aq)}$], which is isotopically lighter due to differences in bond lengths and coordination numbers. Increases in [Ca] at the calcification site during biogenic precipitation could therefore cause the carbonate phase to be isotopically heavier, by increasing the relative proportion of uncharged species (Chen et al., 2017; Chen et al., 2016). It should be emphasised that $\delta^{238}U$ of pelagic biogenic calcites (e.g. foraminifera) have not yet been reported, but in the context of this paper and given the young sample age, if the acetic leachates of ODP758 were only extracting a primary biogenic carbonate phase, we would expect them to have a $\delta^{238}U$ close to, or slightly higher than, modern seawater. The low $\delta^{238}U$ of the acetic leachates in ODP758 instead imply that the majority of carbonate-bound U extracted in ODP758 is not sourced from a primary biogenic precipitate but could instead be from early calcite cements and overgrowths that form as a result of syn-sedimentary diagenesis. This inference is supported by the fact that the bulk carbonate leachates have ~4 times more U (U/Ca = 0.04-0.6 µmol/mol) than has been reported for towline and core top foraminifera (U/Ca = 0.009 – 0.011 µmol/mol) that have undergone oxidative-reductive cleaning and removal of Mn-carbonate overgrowths (Russell et al., 1994). Preferential dissolution of these hypothesised U-enriched cements would also explain the uniform decrease in U/Ca with reductive cleaning, across all leachates in ODP758.

635 The current framework within which early marine diagenesis impacts on U isotopes are interpreted
636 derives exclusively from platform and upper slope settings (Chen et al., 2018a; Romaniello et al., 2013; Tissot
637 et al., 2018). Such sediments contain metastable aragonitic and high-Mg calcite biogenic carbonates in
638 addition to aragonitic and low-Mg calcite cements, in contrast to the more stable low-Mg calcite of pelagic
639 calcifiers and syn-sedimentary cements. In platform settings, diagenesis is typically associated with positive
640 offsets of bulk carbonate compared to seawater (Fig. 3, 5), reflecting changes in U speciation in Ca rich
641 porewaters (Chen et al., 2017; Chen et al., 2016) or the incorporation of reduced (isotopically heavy) U phases
642 as metastable carbonates recrystallize in the presence of sulfidic pore-waters (Chen et al., 2018a; Romaniello
643 et al., 2013). These mechanisms are not consistent with the isotopically light values observed for ODP758 but
644 could explain the isotopic heterogeneity seen in GA183, where the isotopically heavier diagenetic phases may
645 be preferentially leached in the samples that experienced incomplete carbonate dissolution.
646 Contrary to this established framework, all leachates in the Holocene sample produce
647 indistinguishable $\delta^{238}U$ values that are ~0.15‰ lower than seawater, suggesting that the majority of U is
648 instead fixed via adsorption, in a similar manner to clays. Uranyl adsorption onto calcite has been
649 spectroscopically observed in a number of studies (Elzinga et al., 2004; Reeder et al., 2004) and is characterised
650 by the absorption of a charged triscabonate-like uranyl complex, similar to $CaUO_2(CO_3)_3^{2-}$ or $UO_2(CO_3)_3^{4-}$
651 (Elzinga et al., 2004; Reeder et al., 2004). Whilst isotopic fractionation during this process has not been directly
652 measured, it might be expected to exhibit a similar magnitude and direction as adsorption to other minerals
653 with charged functional groups. Indeed, U adsorbed to calcite requires a partial break up of CO_3 groups in the
654 triscarbonate complex, resulting in a measurable distortion of the equatorial oxygen shell (Elzinga et al., 2004;
655 Reeder et al., 2004), possibly equivalent to the loss of symmetry that is invoked to explain the fractionation of
656 U adsorbed to clays and oxides (Brennecka et al., 2011b; Jemison et al., 2016).
657 Although uranyl adsorption to calcite occurs readily, the interaction is relatively weak and uranyl
658 complexes can easily be desorbed due to competition from dissolved uncomplexed CO_3^{2-} and Ca^{2+}
659 (Cumberland et al., 2016; Elzinga et al., 2004; Fox et al., 2006). The high concentration of dissolved carbonate
660 ions in pore-waters would therefore typically promote U mobilization, as is seen in soil environments

(Cumberland et al., 2016). Because of this, a structural stabilization mechanism is still required, and the adsorption of an isotopically light species would only act as an intermediate step before the uranyl complex is fully incorporated. Such a sequence is favoured by Reeder et al., (2004), who suggest that adsorption controls the initial coordination change of uranyl species, but subsequent mineral growth will bury and trap this species, providing a mechanism to incorporate U into calcite and preserve the fractionation induced by adsorption. A similar adsorption mediated incorporation has also recently been suggested for zinc, and may explain the relatively heavy zinc isotopic signature of pelagic carbonates compared to the deep ocean (Dong and Wasylenki, 2016).

The fact that adsorption related isotopic fractionation has not been identified in experimental studies (Chen et al., 2016; Stirling et al., 2015) could be because these experiments do not simulate natural porewater conditions. In particular, the Chen et al., (2016) experiment required extremely high [U] (3600 times seawater) in order to co-precipitate U in calcite in sufficient quantities for isotopic measurement. Elzinga et al., (2004) noted some structural differences in adsorbed U species at higher surface loadings, where at higher concentrations the uranyl complexes were more similar to that directly incorporated into poly-crystalline calcite. Reeder et al., (2004) also show that uranyl incorporation is dictated by the distribution and availability of favourable binding sites. These studies therefore suggest that structural incorporation could be dominant over adsorption in high [U] solutions, and that the precise incorporation mechanism is dependent on the calcite synthesis method. In a natural pelagic sediment sample, primary biogenic calcite also provides a nucleus for secondary calcite cement precipitation, which would act as a surface to promote adsorption. The rapid calcite precipitation that occurs in experimental studies might prevent such surfaces forming, and therefore favour direct co-precipitation of U with no isotopic fractionation. Rapid calcite precipitation could also prevent co-precipitated U from reaching equilibrium (Jemison et al., 2016).

4.4 – Estimated metal isotope budget of a recent carbonate-rich pelagic sediment sample

To summarise the results presented in section 3 and discussion in sections 4.1 – 4.3, the different concentrations and isotopic compositions of the leachates are used to characterise different sedimentary

687 phases with respect to the total sample budget of U and Mo in ODP758 (Fig. 7). Here, the total sample metal
688 budget is represented by the combination of the uncleaned 7M HCl (Fig. 7, Leached) and the associated
689 residue (Fig. 7; Residue). The total metal inventory obtained by combining these two fractions is lower than
690 measured for the total digest (17% and 35% lower for U and Mo, respectively), but this is not unexpected since
691 the leachates and residues underwent multiple washes that would have removed additional clays. The
692 different leachate results are then used to divide the sample into three main components: i) carbonate-bound;
693 ii) Mn-oxide associated; and iii) silicate-bound.

694 Carbonate associated U is represented by the uncleaned buffered acetic acid leachate which
695 demonstrates near-complete dissolution of carbonate, with minimum silicate contributions evident from low
696 Al concentrations. This is further divided into biogenic and syn-sedimentary origin, based on the
697 concentrations from individual foraminifera (Russel et al., 1994), which suggests that only a quarter of the
698 carbonate might be biogenic (section 4.3). The biogenic carbonate fraction is tentatively assumed to record
699 seawater δ^{238}U at -0.40‰ but the remainder of the syn-sedimentary carbonate fraction is -0.55‰, reflecting
700 adsorption mediated U incorporation (section 4.3). For Mo, the carbonate fraction is estimated from the
701 cleaned 1M HCl leachate, which shows the highest δ^{98}Mo and does not suffer from the re-adsorption of Mo
702 onto the residue, as seen in acetic leachates. This is likely an upper estimate of carbonate Mo concentrations
703 (and lower estimate of δ^{98}Mo) as some silicate derived Mo could be present in this leachate. As such, we
704 suggest that carbonate associated Mo is relatively high in δ^{98}Mo (>2.1‰), but it is not possible to constrain
705 this value precisely. The separation of biogenic and syn-sedimentary calcite for Mo is not possible here, due
706 to a lack of primary foraminifera Mo concentration data in the literature.

707 Manganese-oxide contributions for Mo are estimated from the difference between the uncleaned and
708 cleaned 3M HCl leachates, which show the greatest difference in Mo/Ca with reductive cleaning, and are
709 assumed to have a δ^{98}Mo similar to modern Fe-Mn-oxides at -0.6‰ (Siebert et al., 2013). An exchangeable
710 Mo fraction is also likely present and extracted in uncleaned acetic leachates (section 4.1) but it is not possible
711 to quantitatively separate it from the Mn-oxide pool using these leachate data. For U, the Mn-oxide
712 contribution is estimated based on Mo/U of modern Fe-Mn crusts (section 4.1) and assumed to have a δ^{238}U

of -0.6‰ (Goto et al., 2014). A silicate derived fraction for Mo and U is estimated as the difference between the uncleaned 7M HCl leachate and the sum of other phases. For U this is most likely a clay fraction, with a $\delta^{238}U$ of -0.55‰, where the isotopic composition is also driven by adsorption (section 4.2). For Mo the leached silicate fraction has a $\delta^{98}Mo$ close to UCC at ~0.2‰, based on the mixing relationship observed in the cleaned leachates (section 4.2). Importantly, U also has a robust silicate fraction that is not leached and appears to be present in the residue, with a $\delta^{238}U$ similar to BSE at -0.35‰ (section 4.2). By contrast, Mo in the residue appears to be Mn-oxide derived, with a low $\delta^{98}Mo$ of -0.6‰ (section 4.1).

The estimated total sample metal isotope budget is considered only to be semi-quantitative because the leachates were performed on different subsamples, rather than sequentially. Furthermore, the leaching techniques used were not targeted specifically at particular phases, but were primarily designed to assess sample treatment methods that are used for paleo-environmental studies. None-the-less, using these estimates, the calculated $\delta^{238}U$ for the bulk sample is -0.40‰, which agrees well with the measured $\delta^{238}U$ of the total digest (-0.37 $\pm$0.07‰). For Mo, the calculated bulk signature is -0.37‰, which is within error of the measured total digest (-0.29 $\pm$0.10‰). Thus, Figure 7 serves to illustrate the potential contamination of a carbonate signature, where buffered acetic leachates access primarily the carbonate bound phase, and more concentrated acids will attack both silicate and Mn-oxide components. Reductive cleaning removes Mn-oxides, in which case more concentrated acids will attack both carbonate and silicate phases.

4.5 Implications, future work and recommendations for palaeo-redox reconstructions

4.5.1 - Uranium

The $\delta^{238}U$ of the dominant carbonate fraction in pelagic carbonates (calcite) appears to be controlled by adsorption-related isotopic fractionation, in a similar manner to authigenic clays, with both having a $\delta^{238}U$ of ~-0.55‰, i.e. ~0.15‰ lower than seawater. Whilst adsorption related isotope fractionation appears important for calcite in pelagic sediments, it is not clear if this process is prevalent in other types of calcite. In particular, biogenic calcite precipitation seems to be dominated by the effects of local aqueous U speciation at the calcification site, producing $\delta^{238}U$ values slightly higher than seawater (Chen et al., 2018b). Additionally, no

739 isotopic fractionation appears to be involved in the transformation of aragonite to calcite (Chen et al., 2018a)
740 and bulk measurements of recrystallized platform carbonates tend to be dominated by higher $\delta^{238}U$ values,
741 due to the reducing nature of porewaters and U speciation in the presence of Ca (Chen et al., 2018a;
742 Romaniello et al., 2013). Low $\delta^{238}U$ have been reported for a limited number of calcite cements in reef
743 carbonates (Hood et al., 2016) and some speleothem calcite samples (Stirling et al., 2007), which could be
744 evidence for isotopic fraction by adsorption, however interaction with meteoric and burial fluids and
745 groundwater processes could also be important (Hood et al., 2016; Stirling et al., 2007). Further work is
746 therefore required to understand the U isotopic signatures recorded in calcites, and in particular, the
747 importance of adsorption for the $\delta^{238}U$ of pelagic carbonate sediments.

748 The leaching experiments performed here examine potential detrital and Mn-oxide contamination in
749 pelagic calcite sediments with low U concentrations. Such samples have a higher sensitivity to potential
750 contaminants compared to aragonitic sediments that have been the focus of modern studies to date (e.g.
751 Chen et al., 2018b; Romaniello et al., 2013; Tissot et al., 2018). Dilute HCl, HNO_3 and unbuffered 1M acetic
752 acid demonstrably attack non-carbonate components compared to the buffered acetic leachates, including
753 Mn-oxides and silicate minerals, but this does not appear to have a significant impact on $\delta^{238}U$. This result is
754 consistent with the leaching tests of Lau et al., (2016) and Zhang et al., (2018b) who documented
755 indistinguishable $\delta^{238}U$ from a range of acid molarities on higher uranium concentration platform carbonates.
756 This result is somewhat surprising for a low U concentration calcite sample but can be explained here by
757 highlighting three important points. Firstly, in these samples, the Mn-oxide pool of U appears insufficient to
758 affect the mass balance of the leachates and has a similar isotopic composition to the leachable phases.
759 Secondly the main detrital U reservoir in these pelagic sediment samples is in robust, refractory mineral phases
760 and inclusions and is not appreciably accessible by the leaching techniques employed here (Fig. 7). Thirdly, the
761 non-carbonate fraction that can be leached is composed primarily of authigenic U that is mineralogically
762 bound in clays, and has the same adsorption-related fractionation as the majority of the carbonate phase (Fig.
763 7). The pre-depositional loss of U during terrestrial weathering and transport (Carpentier et al., 2013) may be
764 important for creating a detrital phase that is depleted in easily leachable U. However, there have been

765 suggestions that U loss occurs to a lesser degree if the detrital material is sourced from juvenile terrains
766 (Carpentier et al., 2013) implying that some marine sediments could still contain an easily leachable detrital
767 U pool. It is also worth noting that Archean marine sediments could contain more significant and accessible
768 detrital U, as low atmospheric O_2 would prevent the oxidative liberation of U during weathering. The generality
769 of these findings requires further testing for different detrital compositions.

770 The most significant problem for ancient carbonate samples appears to be related to very weak acids.
771 In GA183, anomalously high $\delta^{238}U$ are seen only in the leachates with the lowest U yields (0.2M HCl). This
772 suggests that the problem is either due to the incomplete dissolution of the carbonate, or the re-adsorption
773 of U onto the sample residue. These problems could therefore be avoided by simply using a larger volume of
774 acid to completely dissolve the carbonate and keep metals in solution. The higher $\delta^{238}U$ in the anomalous
775 leachates would be consistent with findings of previous step-wise leaching experiments (Zhang et al., 2018b),
776 which demonstrate isotopic heterogeneities with progressive leaching of ancient carbonate samples that were
777 inferred to represent the differential dissolution of diagenetic phases. Micro-scale variability has also been
778 observed for marine and burial cements in reef carbonates (Hood et al., 2016; Hood et al., 2018). Given the
779 lack of cleaning-derived isotope fractionation, and the lack of isotope fractionation in the incomplete
780 dissolutions of ODP758, we suggest that the differences observed in the 0.2M HCl leachates of GA183 are
781 probably related to isotopic heterogeneity within the sample due to later diagenetic processes. Dedicated
782 studies are required to test this inference, however, a diagenetic origin for the high $\delta^{238}U$ values in GA183
783 would be consistent with the incorporation of U from reducing pore waters during early diagenesis (Chen et
784 al., 2018a; Romaniello et al., 2013) or changes in U speciation in Ca rich pore fluids during burial (Chen et al.,
785 2017; Chen et al., 2018a). Notably, there is no difference in Mn/Sr for these anomalous leachates, which is
786 often relied upon to demonstrate the degree of diagenetic alteration in carbonate samples. The importance
787 of heterogenous carbonate phases will vary with sample type and diagenetic history, but near-complete
788 carbonate dissolution should be ensured with excess acid to avoid any selective leaching-induced artefacts.

789 A pre-dissolution step using weak acid has previously been suggested to remove non-primary
790 carbonate phases (including adsorbed phases and secondary overgrowths) allowing for the better

identification of seawater signatures for rare earth elements (Tostevin et al., 2016) and $\delta^{238}U$ (Tissot et al., 2018) from the remaining carbonate. For U, in both of these samples, it appears that reductive cleaning is equivalent to undertaking partial dissolution as a pre-treatment, but there is no resolvable effect on isotopic compositions. ODP758 shows a uniform decrease in U/Ca across all leachates with reductive cleaning, which could be evidence for the partial removal of early diagenetic cements. By contrast, GA183 does not show such a decrease in U/Ca with cleaning, suggesting the sample has more homogenous concentrations despite isotopic heterogeneity suggested by the 0.2M HCl leachates. This could be the result of later diagenetic stabilization of the sample, and questions the efficacy of pre-leaching as an effective way to avoid diagenetic phases for U in ancient carbonates.

Potential diagenetic offsets have also previously been observed in ancient pelagic chalk samples, where the best preserved samples are ~0.1 – 0.2‰ lower than more lithified chalk samples, and 0.2 – 0.3‰ lower than recrystallized platform samples (Clarkson et al., 2018). This could indicate that diagenetic impacts are less severe in pelagic than platform samples, or it could represent the compounded effect of initial adsorption-dominated U incorporation in syn-sedimentary cements, plus later isotopically heavy U during early burial. All pelagic carbonate sediments will be affected by reducing porewaters during burial, where U(IV) could be incorporated into the carbonate fraction. The net result of these two processes is likely a higher $\delta^{238}U$ than the original seawater (as seen for GA183), but further work is required to address the magnitude and consistency of these changes before invoking a standard diagenetic correction to pelagic sediments, as is often used for platform samples (e.g. Elrick et al., 2017; Zhang et al., 2018b; Zhang et al., 2018c). Although significant for the U budget of the calcite sample analysed here, adsorbed authigenic U is unlikely to be important for predominantly originally aragonitic samples, which form the majority of palaeo-records published to date and contain ppm levels of U. However, adsorption could be important for pelagic sediments, which provide a valuable sedimentary archive for events such as the Paleocene-Eocene Thermal Maxima and OAEs.

Based on these findings, published $\delta^{238}U$ datasets should be comparable, despite using a wide range of acid concentrations and digestion techniques, especially given that the majority of published data come from platform sediments with higher U concentrations. This is consistent with the replication of $\delta^{238}U$ trends

in multiple Permo-Triassic sequences (Zhang et al., 2018). However, even if dilute HCl leachates do not produce resolvable isotopic differences in this study, caution should be applied to using this approach, especially in pelagic carbonates, as even very dilute HCl can liberate U from apatite with very high concentrations (Dahl et al., 2017). Furthermore, additional non-carbonate U liberated by dilute HCl would still influence U/Ca, and hence complicate the use of normalized U concentration and $\delta^{238}U$ covariation to support interpretations of primary seawater trends (e.g. Brennecka et al., 2011a; Clarkson et al., 2018; Tostevin et al., 2019), or the identification of unusual U enrichments or depletions that could be indicative of local diagenetic influences. As such we recommend using an excess buffered acetic acid leaching solution to avoid detrital phases and apatite, yet still ensure complete carbonate dissolution. Due to the limitations of the samples presented here, we urge future studies to test this result by undertaking leaching experiments with different concentrations of acids in an attempt to confirm a lack of isotopic mixing relationships between carbonate and detrital end-members. This is particularly important to test for samples where past seawater is likely to have had a $\delta^{238}U$ signature more fractionated relative to the silicate end-member, such as during intervals of expanded oceanic anoxia.

4.5.2 - Molybdenum

In contrast to U, Mo displays extreme sensitivity to exchangeable, detrital and Mn-oxide bound contaminants, consistent with previous findings (Siebert et al., 2003). This makes it difficult to isolate the pure carbonate phase, and hence the precise relationship of pelagic carbonates to seawater signatures remains poorly constrained. None-the-less, the carbonate phase appears to be relatively isotopically heavy. Further work is required to constrain the relationship of carbonates to seawater but the experiments presented here demonstrate two important points: i) Mn-oxide and exchangeable Mo must be removed from the sample to isolate the carbonate fraction as these phases are accessible to even very dilute acids and can significantly impact the $\delta^{98}Mo$ of a leachate; ii) there is a strong influence of silicate minerals and clays on the measured $\delta^{98}Mo$ of the leachate. An additional complication for Mo comes from the potential re-adsorption of Mo onto clays in acetic acid based leachates that are traditionally considered for selective carbonate dissolution.

843 Tentatively, a short duration dilute HCl leach, after reductive cleaning, appears the most successful for
844 isolating seawater signatures in pelagic carbonates, but sample heterogeneity controls the abundance of
845 detrital minerals and affects the measured δ^{98}Mo. As such, future work should focus on the purest carbonate
846 sediments and/or develop a robust method to remove clay contaminants, in addition to removing Mn-oxide
847 phases.

848 Whilst acknowledging that the pelagic carbonate sample is different to other published carbonate sample
849 types, the Mn-oxide contribution of Mo may have been overlooked by previous studies of δ^{98}Mo in both
850 modern and ancient carbonates. Modern non-biogenic carbonate samples from oxic settings have been
851 suggested to record close-to-seawater δ^{98}Mo compositions, although the range of values is still large, even
852 after detrital correction (1.10 – 2.19‰) (Voegelin et al., 2009). By contrast, even greater variability and lighter
853 isotopic compositions (0.07 – 2.12‰) were identified for skeletal carbonate sands, which were interpreted to
854 reflect a 'vital effect' control on skeletal δ^{98}Mo (Voegelin et al., 2009). Relatively low δ^{98}Mo have also been
855 observed for Bahamas bulk carbonate samples (Romaniello et al., 2016), modern stromatolites and
856 thrombolites (Thoby et al., 2019). The scatter in these datasets may be partially explained by Mo speciation
857 and the degree of quantitative Mo removal in porewaters (Romaniello et al., 2016; Thoby et al., 2019), and
858 silicate contributions from detrital minerals (Thoby et al., 2019; Voegelin et al., 2010; Voegelin et al., 2009).
859 But, as these studies utilized relatively concentrated acid leachates (3N HCl and 6.4N HCl) without pre-cleaning
860 treatments, it is also likely that a significant Fe-Mn-oxide Mo pool is present in the samples, contributing to
861 isotopically lighter bulk values. Thus, the reductive cleaning tests presented here suggest that the δ^{98}Mo of
862 carbonates requires further examination. That said, the Bahamas ooid samples, run here as a secondary
863 standard, do not show any difference with reductive cleaning.

864 From the perspective of paleo-redox reconstructions, it is likely that Mo isotope signatures from ancient
865 carbonates leached using strong mineral acids (e.g. Eroglu et al., 2015; Thoby et al., 2019; Voegelin et al., 2010;
866 Voegelin et al., 2009) will represent a mixture of Mn-oxide-derived, detrital and carbonate components in
867 addition to residual organic matter. The relative abundance of these components will vary by sample, even
868 within the same lithology, thereby making interpretation of secular trends difficult and likely affected by local

depositional conditions. Furthermore, the dominance of the Mn-oxide fraction in carbonate sediments, and their residues, suggests that it is not appropriate to rely on UCC-based detrital corrections for leachates, as has been done previously (Voegelin et al., 2010; Voegelin et al., 2009). Finally, whatever signature is captured by a carbonate in the oxic sedimentary zone must then pass through deeper zones of reduction and diagenesis that will likely modify the signature. The primary Mn-oxide or exchangeable fractions will change due to later diagenetic stabilization and/or the reductive loss of Mn-oxides. Molybdenum associated with these phases could be incorporated into more stable Fe-Mn minerals, transferred to diagenetic carbonate phases or lost to the water column. The fate of Mo during these diagenetic transformations requires further investigation, but has very significant implications for the recorded isotope signatures extracted by different leaching techniques, and the utility of δ^{98}Mo in carbonates. It has also been suggested that the best ancient carbonates to target for δ^{98}Mo would be those that demonstrate evidence for the presence of pore water sulfide during early diagenesis (Romaniello et al., 2016). This may enable near quantitative Mo drawdown by secondary carbonate precipitates, in a manner that preserves seawater signatures as in euxinic shales, but this would certainly lead to greater alteration of δ^{238}U in the same sample. For ancient samples, it is also difficult to definitively state whether pore-waters were persistently euxinic or not, and whether Mo drawdown was indeed quantitative.

5 - Conclusion

The Holocene sample studied here provides important constraints on the relationship of bulk pelagic carbonates to seawater. For U, we suggest that the bulk carbonate δ^{238}U signature is dominated by adsorption-related fractionation during syn-sedimentary carbonate cementation, producing a negative fractionation relative to seawater of ~-0.15‰. The prevalence of this process in the global ocean requires further examination, as does the preservation of this signature during burial. For Mo, the mixing relationship identified in reductively cleaned samples suggests that the pure carbonate phase is relatively isotopically heavy. We cannot, however, constrain the precise relationship to seawater and dedicated studies are required to do this, utilizing reductive cleaning and selective leaching methods to discount Mn-oxide and silicate influences. Like

U, it is possible that the carbonate δ^{98}Mo signature is acquired during syn-sedimentary carbonate cementation in pelagic settings, rather than being purely primary in origin.

More generally, metal isotopes are increasingly being used for paleo-environmental reconstructions during key intervals of Earth history, and carbonates are a favoured archive. As these measurements become more common, it is critical to ensure that the methods used are comparable and truly representative of carbonate. In addition to standardized approaches for chemical purification, isotope measurement protocols and data reporting, it is important to use sediment digestion techniques that can be widely adopted and applied to a variety of sediments types, secure in the knowledge that the chosen method will not introduce bias or artefacts into geochemical records.

The study presented here examines the efficacy of reductive cleaning and selective leaching protocols for U and Mo isotopes in pelagic carbonate sediments, and demonstrates an effective experimental approach that can be applied to other metal isotope systems and other sediment types. Through cleaned and uncleaned sample pairs, leached via a range of acid concentrations, the potential for detrital or Mn-oxide bound contamination can be robustly identified. For Mo, variability in the leachates indicates a high potential for measurements to be biased by non-carbonate components. This would make it very difficult to robustly interpret secular changes through time, even using the same lithology, when no reductive cleaning measures are undertaken and more concentrated acids are used for leaching. For U, the impacts seem to be less dramatic, but care needs to be taken to ensure complete digestion. Thus, the impact of contaminant components clearly varies for different metal isotope systems, and we urge future palaeo-studies to undertake similar tests on different sample types in order to better understand the success of isolating carbonate-bound metals for isotopic measurements.

Acknowledgments

This project has received funding from the European Union's Horizon 2020 research and innovation programme under the Marie Sklodowska-Curie grant agreement No 795722 and Swiss SNF grants

200020_165904 and 200021_184873. Thanks to Kevin Burton, Brandi Revels, Marion Garcon and Netta Shalev for helpful discussions, and Corey Archer and Emily Ciscato for laboratory assistance. This paper benefited significantly from the inputs of Stephen Romaniello and an anonymous reviewer.

Data Availability

Data related to this paper are available from the ETHZ research collection at https://www.research-collection.ethz.ch/handle/20.500.11850/380187

930 **References**

931 Alam, M.S., Cheng, T., 2014. Uranium release from sediment to groundwater: Influence of water chemistry
932 and insights into release mechanisms. Journal of Contaminant Hydrology, 164: 72-87.
933 Andersen, M. et al., 2014. A modern framework for the interpretation of $^{238}U/^{235}U$ in studies of ancient
934 ocean redox. Earth and Planetary Science Letters, 400: 184–94.
935 Andersen, M., Stirling, C., Zimmermann, B., Halliday, A., 2010. Precise determination of the open ocean
936 234U/238U composition. Geochemistry, Geophysics, Geosystems, 11(12).
937 Andersen, M., Stirling, C.H., Weyer, S., 2017. Uranium isotope fractionation. Rev. Mineral. Geochem, 82(1):
938 799–850.
939 Andersen, M. et al., 2016. Closing in on the marine $^{238}U/^{235}U$ budget. Chemical Geology, 420: 11–22.
940 Andersen, M.B. et al., 2015. The terrestrial uranium isotope cycle. Nature, 517(7534): 356–359.
941 Andersen, M.B., Erel, Y., Bourdon, B., 2009. Experimental evidence for $^{234}U–^{238}U$ fractionation during granite
942 weathering with implications for 234U/238U in natural waters. Geochimica et Cosmochimica Acta,
943 73(14): 4124-4141.
944 Archer, C., Vance, D., 2008. The isotopic signature of the global riverine molybdenum flux and anoxia in the
945 ancient oceans. Nature Geoscience, 1(9): 597.
946 Arnold, G.L., Anbar, A., Barling, J., Lyons, T., 2004. Molybdenum isotope evidence for widespread anoxia in
947 mid-Proterozoic oceans. Science, 304(5667): 87-90.
948 Barling, J., Anbar, A., 2004. Molybdenum isotope fractionation during adsorption by manganese oxides.
949 Earth and Planetary Science Letters, 217(3-4): 315-329.
950 Barling, J., Arnold, G.L., Anbar, A., 2001. Natural mass-dependent variations in the isotopic composition of
951 molybdenum. Earth and Planetary Science Letters, 193(3-4): 447-457.
952 Barnes, C.E., Cochran, J.K., 1993. Uranium geochemistry in estuarine sediments: controls on removal and
953 release processes. Geochimica et Cosmochimica Acta, 57(3): 555-569.
954 Bartlett, R. et al., 2018. Abrupt global-ocean anoxia during the Late Ordovician–early Silurian detected using
955 uranium isotopes of marine carbonates. Proceedings of the National Academy of Sciences, 115(23):
956 5896-5901.
957 Bian, N., Martin, P.A., 2010. Investigating the fidelity of Mg/Ca and other elemental data from reductively
958 cleaned planktonic foraminifera. Paleoceanography, 25.
959 Blichert-Toft, J., Zanda, B., Ebel, D.S., Albarède, F., 2010. The solar system primordial lead. Earth and
960 Planetary Science Letters, 300(1-2): 152-163.
961 Bomou, B. et al., 2013. The expression of the Cenomanian–Turonian oceanic anoxic event in Tibet.
962 Palaeogeography, Palaeoclimatology, Palaeoecology, 369: 466-481.

963 Boyle, E., Keigwin, L., 1985. Comparison of Atlantic and Pacific paleochemical records for the last 215,000
964 years: Changes in deep ocean circulation and chemical inventories. Earth and Planetary Science
965 Letters, 76(1-2): 135-150.
966 Boyle, E.A., 1983. Manganese carbonate overgrowths on foraminifera tests. Geochimica et Cosmochimica
967 Acta, 47(10): 1815-1819.
968 Brennecka, G.A., Herrmann, A.D., Algeo, T.J., Anbar, A.D., 2011a. Rapid expansion of oceanic anoxia
969 immediately before the end-Permian mass extinction. Proceedings of the National Academy of
970 Sciences of the United States of America, 108(43): 17631–17634.
971 Brennecka, G.A., Wasylenki, L.E., Bargar, J.R., Weyer, S., Anbar, A.D., 2011b. Uranium Isotope Fractionation
972 during Adsorption to Mn-Oxyhydroxides. Environmental Science & Technology, 45(4): 1370-1375.
973 Bura-Nakić, E. et al., 2018. Coupled Mo-U abundances and isotopes in a small marine euxinic basin:
974 constraints on processes in euxinic basins. Geochimica et Cosmochimica Acta, 222: 212-229.
975 Burton, K.W., Vance, D., 2000. Glacial–interglacial variations in the neodymium isotope composition of
976 seawater in the Bay of Bengal recorded by planktonic foraminifera. Earth and Planetary Science
977 Letters, 176(3-4): 425-441.
978 Carpentier, M., Weis, D., Chauvel, C., 2013. Large U loss during weathering of upper continental crust: the
979 sedimentary record. Chemical Geology, 340: 91-104.
980 Chen, X., Romaniello, S.J., Anbar, A.D., 2017. Uranium isotope fractionation induced by aqueous speciation:
981 Implications for U isotopes in marine $CaCO_3$ as a paleoredox proxy. Geochimica et Cosmochimica
982 Acta, 215: 162-172.
983 Chen, X. et al., 2018a. Diagenetic effects on uranium isotope fractionation in carbonate sediments from the
984 Bahamas. Geochimica et Cosmochimica Acta, 237: 294-311.
985 Chen, X., Romaniello, S.J., Herrmann, A.D., Samankassou, E., Anbar, A.D., 2018b. Biological effects on
986 uranium isotope fractionation ($^{238}U/^{235}U$) in primary biogenic carbonates. Geochimica et
987 Cosmochimica Acta, 240: 1-10.
988 Chen, X., Romaniello, S.J., Herrmann, A.D., Wasylenki, L.E., Anbar, A.D., 2016. Uranium isotope fractionation
989 during coprecipitation with aragonite and calcite. Geochimica et Cosmochimica Acta, 188: 189–207.
990 Clarkson, M.O. et al., 2018. Uranium isotope evidence for two episodes of deoxygenation during Oceanic
991 Anoxic Event 2. Proceedings of the National Academy of Sciences, 115(12): 2918-2923.
992 Conway, T.M., Rosenberg, A.D., Adkins, J.F., John, S.G., 2013. A new method for precise determination of
993 iron, zinc and cadmium stable isotope ratios in seawater by double-spike mass spectrometry.
994 Analytica chimica acta, 793: 44-52.
995 Cumberland, S.A., Douglas, G., Grice, K., Moreau, J.W., 2016. Uranium mobility in organic matter-rich
996 sediments: A review of geological and geochemical processes. Earth-Science Reviews, 159: 160-185.

997 Dahl, T.W. et al., 2014. Uranium isotopes distinguish two geochemically distinct stages during the later
998 Cambrian SPICE event. Earth and planetary science letters, 401: 313–326.
999 Dahl, T.W. et al., 2017. Reorganisation of Earth's biogeochemical cycles briefly oxygenated the oceans 520
1000 Myr ago. Geochemical Perspectives, 3: 210-220.
1001 Dickson, A., 2017. A molybdenum isotope perspective on Phanerozoic deoxygenation events.
1002 Dong, S., Wasylenki, L.E., 2016. Zinc isotope fractionation during adsorption to calcite at high and low ionic
1003 strength. Chemical Geology, 447: 70-78.
1004 Duan, Y. et al., 2010. Molybdenum isotope evidence for mild environmental oxygenation before the Great
1005 Oxidation Event. Geochimica et Cosmochimica Acta, 74(23): 6655-6668.
1006 Dunk, R., Mills, R., Jenkins, W., 2002. A reevaluation of the oceanic uranium budget for the Holocene.
1007 Chemical Geology, 190(1): 45–67.
1008 Elrick, M. et al., 2017. Global-ocean redox variation during the middle-late Permian through Early Triassic
1009 based on uranium isotope and Th/U trends of marine carbonates. Geology, 45(2): 163-166.
1010 Elzinga, E.J. et al., 2004. Spectroscopic investigation of U(VI) sorption at the calcite-water interface.
1011 Geochimica et Cosmochimica Acta, 68(11): 2437-2448.
1012 Eroglu, S., Schoenberg, R., Wille, M., Beukes, N., Taubald, H., 2015. Geochemical stratigraphy,
1013 sedimentology, and Mo isotope systematics of the ca. 2.58–2.50Ga-old Transvaal Supergroup
1014 carbonate platform, South Africa. Precambrian Research, 266: 27-46.
1015 Fox, P.M., Davis, J.A., Zachara, J.M., 2006. The effect of calcium on aqueous uranium (VI) speciation and
1016 adsorption to ferrihydrite and quartz. Geochimica et Cosmochimica Acta, 70(6): 1379-1387.
1017 Froelich, P.N. et al., 1979. Early oxidation of organic matter in pelagic sediments of the eastern equatorial
1018 Atlantic: suboxic diagenesis. Geochimica et cosmochimica acta, 43(7): 1075-1090.
1019 Goldberg, S., Forster, H., Godfrey, C., 1996. Molybdenum adsorption on oxides, clay minerals, and soils. Soil
1020 Science Society of America Journal, 60(2): 425-432.
1021 Goto, K.T. et al., 2014. Uranium isotope systematics of ferromanganese crusts in the Pacific Ocean:
1022 Implications for the marine $^{238}U/^{235}U$ isotope system. Geochimica et Cosmochimica Acta, 146: 43-58.
1023 Hirst, D., Nicholls, G., 1958. Techniques in sedimentary geochemistry:(1) Separation of the detrital and non-
1024 detrital fractions of limestones. Journal of Sedimentary Research, 28(4).
1025 Hood, A.v. et al., 2016. Integrated geochemical-petrographic insights from component-selective δ238U of
1026 Cryogenian marine carbonates. Geology, 44(11): 935–938.
1027 Hood, A.v.S., Planavsky, N.J., Wallace, M.W., Wang, X., 2018. The effects of diagenesis on geochemical
1028 paleoredox proxies in sedimentary carbonates. Geochimica et Cosmochimica Acta, 232: 265-287.
1029 Ivanovich, M., Harmon, R., 1992. Uranium-series disequilibrium: applications to earth, marine and
1030 environmental sciences. 2" ed. Clarendon Press, Oxford.

1031 Jemison, N.E., Johnson, T.M., Shiel, A., Lundstrom, C.C., 2016. Uranium isotopic fractionation induced by U
1032 (VI) adsorption onto common aquifer minerals. Environmental science & technology, 50(22): 12232-
1033 12240.
1034 John, S.G., Kunzmann, M., Townsend, E.J., Rosenberg, A.D., 2017. Zinc and cadmium stable isotopes in the
1035 geological record: A case study from the post-snowball Earth Nuccaleena cap dolostone.
1036 Palaeogeography, Palaeoclimatology, Palaeoecology, 466: 202-208.
1037 Jost, A.B. et al., 2017. Uranium isotope evidence for an expansion of marine anoxia during the end-Triassic
1038 extinction. Geochemistry, Geophysics, Geosystems.
1039 Kendall, B., Dahl, T.W., Anbar, A.D., 2017. The stable isotope geochemistry of molybdenum. Reviews in
1040 Mineralogy and Geochemistry, 82(1): 683-732.
1041 Kendall, B., Gordon, G.W., Poulton, S.W., Anbar, A.D., 2011. Molybdenum isotope constraints on the extent
1042 of late Paleoproterozoic ocean euxinia. Earth and Planetary Science Letters, 307(3-4): 450-460.
1043 Koschinsky, A., Halbach, P., 1995. Sequential leaching of marine ferromanganese precipitates: Genetic
1044 implications. Geochimica et Cosmochimica Acta, 59(24): 5113-5132.
1045 Koschinsky, A., Hein, J.R., 2003. Uptake of elements from seawater by ferromanganese crusts: solid-phase
1046 associations and seawater speciation. Marine Geology, 198(3-4): 331-351.
1047 Kunzmann, M. et al., 2013. Zn isotope evidence for immediate resumption of primary productivity after
1048 snowball Earth. Geology, 41(1): 27-30.
1049 Lau, K.V., Macdonald, F.A., Maher, K., Payne, J.L., 2017. Uranium isotope evidence for temporary ocean
1050 oxygenation in the aftermath of the Sturtian Snowball Earth. Earth and Planetary Science Letters,
1051 458: 282-292.
1052 Lau, K.V. et al., 2016. Marine anoxia and delayed Earth system recovery after the end-Permian extinction.
1053 Proceedings of the National Academy of Sciences, 113(9): 2360–2365.
1054 Leventhal, J., Taylor, C., 1990. Comparison of methods to determine degree of pyritization. Geochimica et
1055 Cosmochimica Acta, 54(9): 2621-2625.
1056 Li, Y.-X., Montañez, I.P., Liu, Z., Ma, L., 2017. Astronomical constraints on global carbon-cycle perturbation
1057 during Oceanic Anoxic Event 2 (OAE2). Earth and Planetary Science Letters, 462: 35-46.
1058 Littke, R., Rullkötter, J., Schaefer, R.G., 1991. Organic and carbonate carbon accumulation on Broken Ridge
1059 and Ninetyeast Ridge, Central Indian Ocean. Proceedings of the Ocean Drilling Program, Scientific
1060 Results, 121.

1061 Martin, P.A., Lea, D.W., 2002. A simple evaluation of cleaning procedures on fossil benthic foraminiferal
1062 Mg/Ca. Geochemistry, Geophysics, Geosystems, 3(10): 1–8.
1063 McKee, B.A., DeMaster, D.J., Nittrouer, C.A., 1987. Uranium geochemistry on the Amazon shelf: evidence for
1064 uranium release from bottom sediments. Geochimica et Cosmochimica Acta, 51(10): 2779-2786.

McLennan, S.M., Taylor, S., 1980. Th and U in sedimentary rocks: crustal evolution and sedimentary recycling. Nature, 285(5767): 621.

Morford, J.L., Emerson, S., 1999. The geochemistry of redox sensitive trace metals in sediments. Geochimica et Cosmochimica Acta, 63(11): 1735–1750.

Morford, J.L., Martin, W.R., Carney, C.M., 2009. Uranium diagenesis in sediments underlying bottom waters with high oxygen content. Geochimica et Cosmochimica Acta, 73(10): 2920–2937.

Nägler, T.F. et al., 2014. Proposal for an International Molybdenum Isotope Measurement Standard and Data Representation. Geostandards and Geoanalytical Research, 38(2): 149-151.

Pagel, M., 1982. The mineralogy and geochemistry of uranium, thorium, and rare-earth elements in two radioactive granites of the Vosges, France. Mineralogical Magazine, 46(339): 149-161.

Peirce, J., Weissel, J., 1989. Proceedings of the Ocean Drilling Program, 121 Initial Reports, College Station, TX.

Pena, L., Calvo, E., Cacho, I., Eggins, S., Pelejero, C., 2005. Identification and removal of Mn-Mg-rich contaminant phases on foraminiferal tests: Implications for Mg/Ca past temperature reconstructions. Geochemistry, Geophysics, Geosystems, 6(9).

Pichat, S., Douchet, C., Albarède, F., 2003. Zinc isotope variations in deep-sea carbonates from the eastern equatorial Pacific over the last 175 ka. Earth and Planetary Science Letters, 210(1-2): 167-178.

Raiswell, R., Canfield, D.E., Berner, R.A., 1994. A comparison of iron extraction methods for the determination of degree of pyritisation and the recognition of iron-limited pyrite formation. Chemical Geology, 111(1-4): 101-110.

Reeder, R.J. et al., 2004. Site-specific incorporation of uranyl carbonate species at the calcite surface. Geochimica et Cosmochimica Acta, 68(23): 4799-4808.

Reeder, R.J. et al., 2001. Coprecipitation of Uranium(VI) with Calcite: XAFS, micro-XAS, and luminescence characterization. Geochimica et Cosmochimica Acta, 65(20): 3491-3503.

Richter, S. et al., 2008. The isotopic composition of natural uranium samples—Measurements using the new n (233U)/n (236U) double spike IRMM-3636. International Journal of Mass Spectrometry, 269(1-2): 145-148.

Romaniello, S.J., Herrmann, A.D., Anbar, A.D., 2013. Uranium concentrations and $^{238}U/^{235}U$ isotope ratios in modern carbonates from the Bahamas: Assessing a novel paleoredox proxy. Chemical Geology, 362: 305–316.

Romaniello, S.J., Herrmann, A.D., Anbar, A.D., 2016. Syndepositional diagenetic control of molybdenum isotope variations in carbonate sediments from the Bahamas. Chemical Geology, 438: 84-90.

Russell, A.D., Emerson, S., Nelson, B.K., Erez, J., Lea, D.W., 1994. Uranium in foraminiferal calcite as a recorder of seawater uranium concentrations. Geochimica et Cosmochimica Acta, 58(2): 671-681.

1099 Siebert, C., Nägler, T.F., von Blanckenburg, F., Kramers, J.D., 2003. Molybdenum isotope records as a
1100 potential new proxy for paleoceanography. Earth and Planetary Science Letters, 211(1-2): 159-171.
1101 Stirling, C.H., Andersen, M.B., Potter, E.-K., Halliday, A.N., 2007. Low-temperature isotopic fractionation of
1102 uranium. Earth and Planetary Science Letters, 264(1): 208–225.
1103 Stirling, C.H., Andersen, M.B., Warthmann, R., Halliday, A.N., 2015. Isotope fractionation of ^{238}U and ^{235}U
1104 during biologically-mediated uranium reduction. Geochimica et Cosmochimica Acta, 163: 200–218.
1105 Tessier, A., Campbell, P.G., Bisson, M., 1979. Sequential extraction procedure for the speciation of
1106 particulate trace metals. Analytical chemistry, 51(7): 844–851.
1107 Thoby, M. et al., 2019. Global importance of oxic molybdenum sinks prior to 2.6 Ga revealed by the Mo
1108 isotope composition of Precambrian carbonates. Geology.
1109 Tieh, T.T., Ledger, E.B., Rowe, M.W., 1980. Release of uranium from granitic rocks during in situ weathering
1110 and initial erosion (central Texas). Chemical Geology, 29(1-4): 227-248.
1111 Tissot, F.L. et al., 2018. Controls of eustasy and diagenesis on the 238U/235U of carbonates and evolution of
1112 the seawater ($^{234}U/^{238}U$) during the last 1.4 Myr. Geochimica et Cosmochimica Acta, 242: 233-265.
1113 Tostevin, R. et al., 2019. Uranium isotope evidence for an expansion of anoxia in terminal Ediacaran oceans.
1114 Earth and Planetary Science Letters, 506: 104-112.
1115 Tostevin, R. et al., 2016. Effective use of cerium anomalies as a redox proxy in carbonate-dominated marine
1116 settings. Chemical Geology, 438(Supplement C): 146-162.
1117 Tribovillard, N., Algeo, T.J., Lyons, T., Riboulleau, A., 2006. Trace metals as paleoredox and paleoproductivity
1118 proxies: an update. Chemical geology, 232(1-2): 12-32.
1119 Voegelin, A.R., Nägler, T.F., Beukes, N.J., Lacassie, J.P., 2010. Molybdenum isotopes in late Archean
1120 carbonate rocks: implications for early Earth oxygenation. Precambrian Research, 182(1): 70-82.
1121 Voegelin, A.R., Nägler, T.F., Samankassou, E., Villa, I.M., 2009. Molybdenum isotopic composition of modern
1122 and Carboniferous carbonates. Chemical Geology, 265(3): 488-498.
1123 Wasylenki, L.E., Rolfe, B.A., Weeks, C.L., Spiro, T.G., Anbar, A.D., 2008. Experimental investigation of the
1124 effects of temperature and ionic strength on Mo isotope fractionation during adsorption to
1125 manganese oxides. Geochimica et Cosmochimica Acta, 72(24): 5997-6005.
1126 Weyer, S. et al., 2008. Natural fractionation of $^{238}U/^{235}U$. Geochimica et Cosmochimica Acta, 72(2): 345-359.
1127 White, D.A., Elrick, M., Romaniello, S., Zhang, F., 2018. Global seawater redox trends during the Late
1128 Devonian mass extinction detected using U isotopes of marine limestones. Earth and Planetary
1129 Science Letters, 503: 68-77.
1130 Zhang, F. et al., 2018a. Global-ocean redox variations across the Smithian-Spathian boundary linked to
1131 concurrent climatic and biotic changes. Earth-Science Reviews.

Zhang, F. et al., 2018b. Congruent Permian-Triassic $\delta^{238}U$ records at Panthalassic and Tethyan sites: Confirmation of global-oceanic anoxia and validation of the U-isotope paleoredox proxy. Geology, 46(4): 327-330.

Zhang, F. et al., 2018c. Multiple episodes of extensive marine anoxia linked to global warming and continental weathering following the latest Permian mass extinction. Science advances, 4(4): e1602921.

Zhang, F. et al., 2018d. Extensive marine anoxia during the terminal Ediacaran Period. Science advances, 4(6): eaan8983.

1142

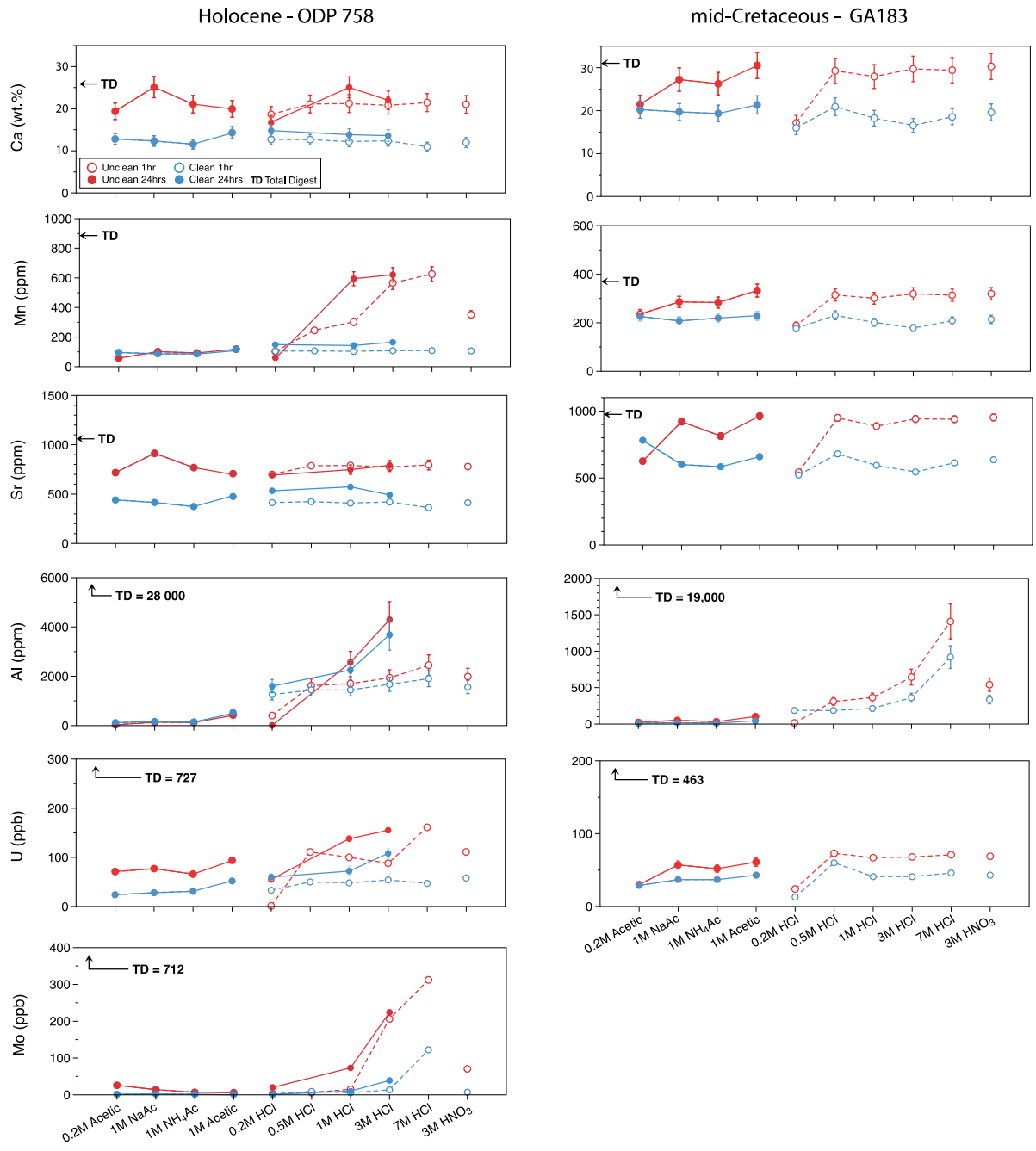

Figure 1: Comparison of major elements across different leaching solutions. Leachates that were left for 24hrs are denoted by solid symbols and a solid line and 1 hr leachates by open symbols and a dashed line. Samples without reductive cleaning are shown in red, and cleaned samples in blue. Concentrations of total digests (TD) are also shown for reference. NaAc = sodium acetate, NH_4Ac = ammonium acetate.

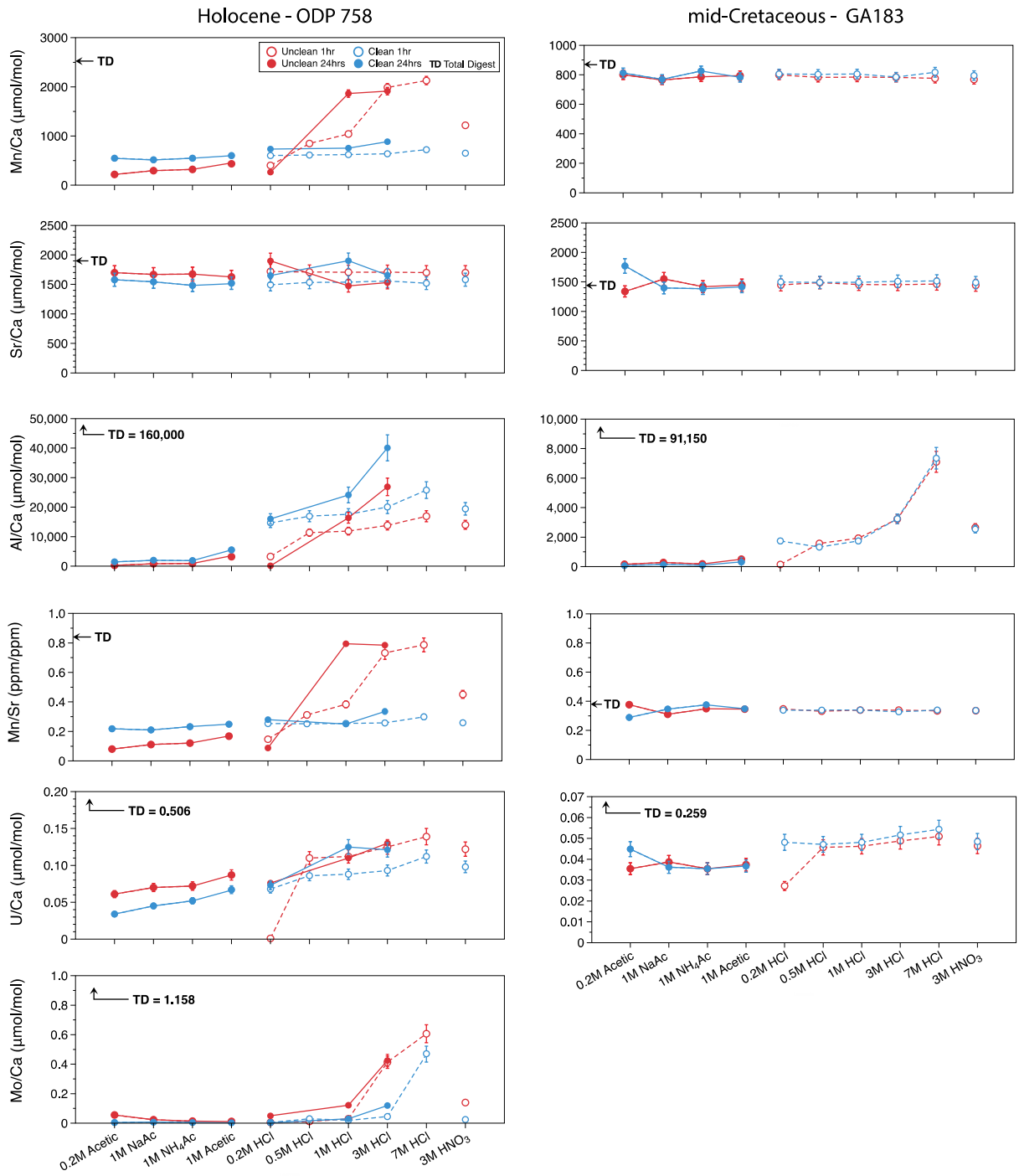

Figure 2: Element/Ca ratios for selected metals. NaAc = sodium acetate, NH_4Ac = ammonium acetate.

1143

1144

1145

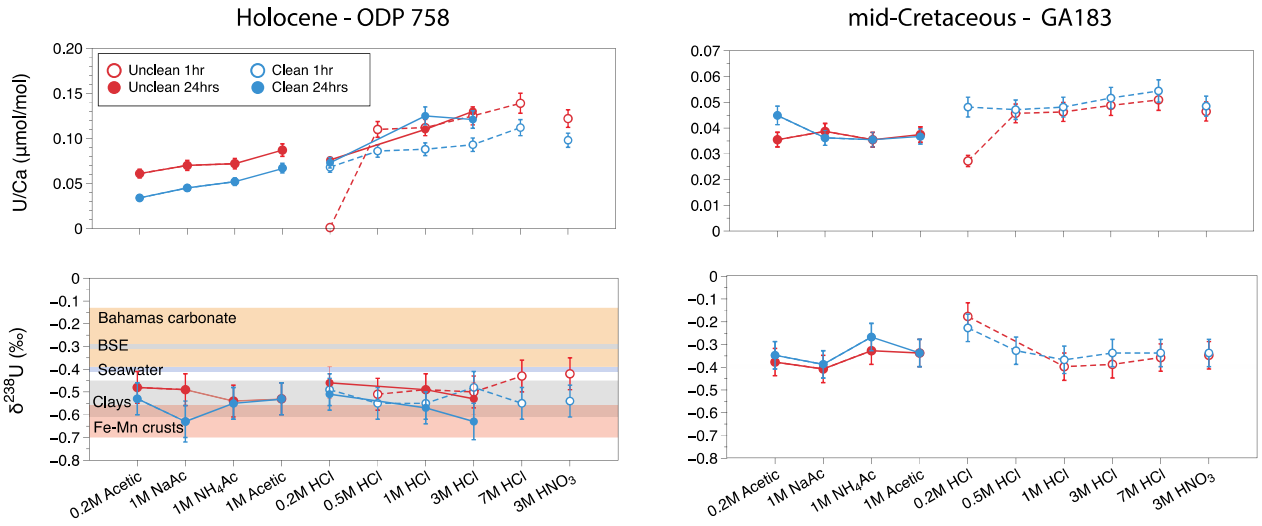

Figure 3: Comparison of U/Ca (upper) and $\delta^{238}U$ (lower) across different leaching solutions. Average $\delta^{238}U$ compositions for Bulk Silicate Earth (BSE) (Andersen et al., 2017), Bahamas carbonates (Chen et al., 2018a), seawater (Andersen et al., 2017) and Fe-Mn crusts (Goto et al., 2014) are shown for the Holocene sample only. The expected $\delta^{238}U$ composition of clays is taken from U adsorbed to clays, quartz and aquifer material (Jemison et al., 2016). NaAc = sodium acetate, NH_4Ac = ammonium acetate.

1146

1147

1148

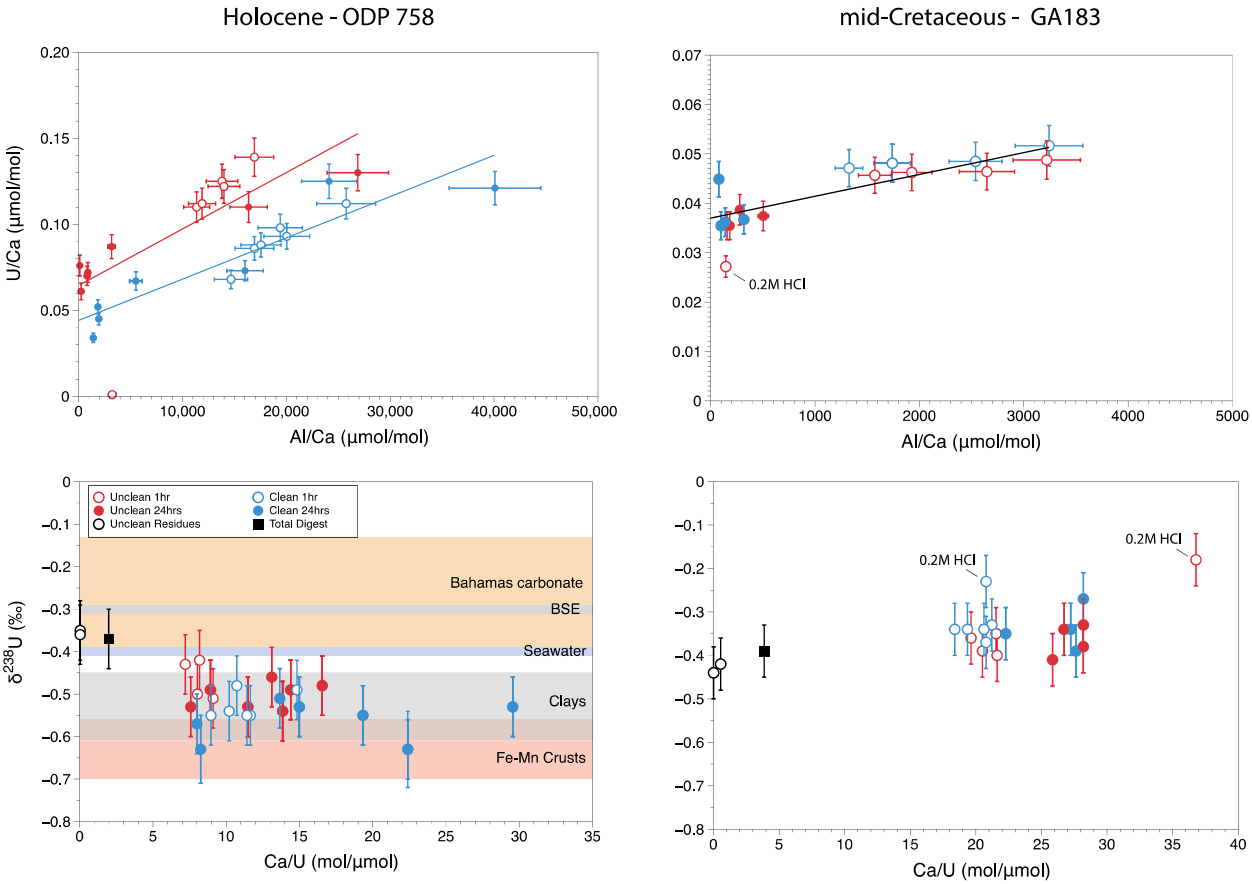

Figure 4: Examination of mixing relationships for U concentrations and $\delta^{238}U$. Best fit lines for U/Ca versus Al/Ca are for cleaned and uncleaned samples of ODP758, and all samples except the 0.2M HCl leachates for GA183. Non-carbonate U contributions can clearly be identified from correlated U/Ca and Al/Ca where the acetic based leachates have lowest U/Ca and Al/Ca. Despite this, no clear variation is seen for $\delta^{238}U$.

1149

1150

1151

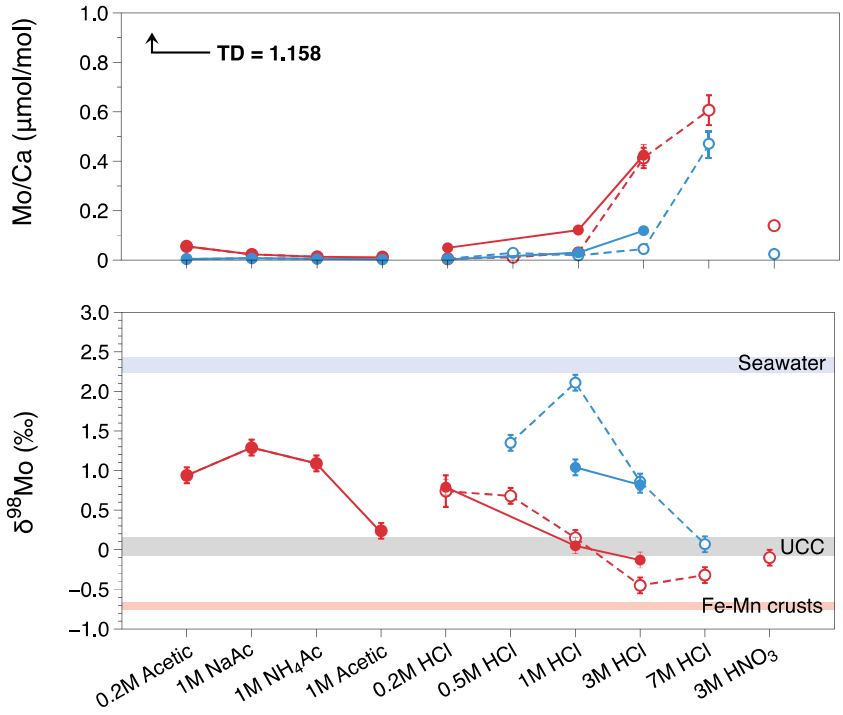

Figure 5: Comparison of Mo/Ca and δ^{98}Mo for each leachate in ODP758. Average values for seawater, Upper Continental Crust (UCC) and Fe-Mn crusts (Siebert et al., 2003) are shown for reference. NaAc = sodium acetate, NH_4Ac = ammonium acetate.

1152

1153

1154

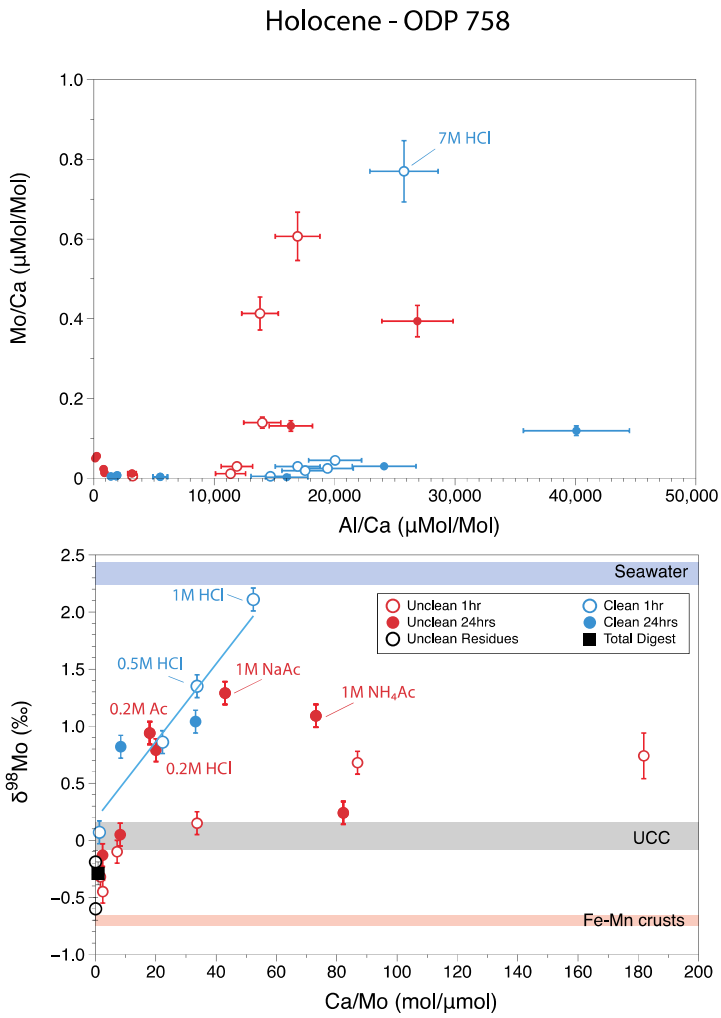

Figure 6: Examination of mixing relationships for Mo concentrations and isotopes. Uncleaned samples show higher Mo concentrations and lower δ^{98}Mo, indicative of Mn-oxide influences. When cleaned, leachates produce a mixing line (blue line) that extends, isotopically, between the cleaned 1 hr 1M HCl leachate, with high δ^{98}Mo, close to the seawater composition, and the cleaned 1 hr 7M HCl leachate with a δ^{98}Mo similar to the upper continental crust (UCC) composition. Some of the uncleaned acetic acid leachates (labelled) show unusually high δ^{98}Mo for their Ca/Mo, suggestive of re-adsorption of Mo onto the sample residue from the leaching solutions.

1155

1156

1157

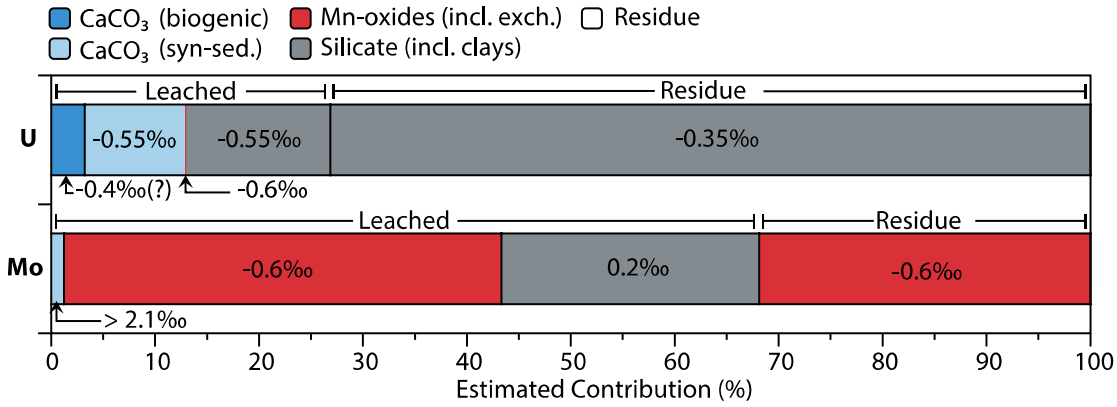

Figure 7: Estimated contributions of different mineralogical fractions for Mo and U in ODP758. The total sample is composed of the 'leached' and 'residue' fractions where the leached phases are: i) carbonate bound (including biogenic and syn-sedimentary); ii) Mn-oxide bound and exchangeable phases; and iii) silicate bound (including clay). The residues appear to mainly contain U in robust silicate minerals and Mo in Mn-oxides. Estimated contributions and isotopic composition of each fraction are made using different leachate data as discussed in section 4.4

1158

1159

1160

Table 1: Acid strength and volumes used for leaching experiments, with pH measurement before and after leaching. Each separate leachate was applied to a reductively cleaned and uncleaned sample pair.

Acid	Volume (ml)	Time (hrs)	pH start	pH end
0.2 M acetic acid	10	24	3	6
1 M sodium acetate	10	24	5	5
1 M ammonium acetate	10	24	5	5
1 M acetic acid	10	24	2.8	4
0.2 M HCl	10	1 & 24	0.7	3.1
0.5 M HCl	7	1	0.3	0.5
1 M HCl	5	1 & 24	0	0.4
3 M HCl	5	1 & 24	0	0.1
7 M HCl	5	1	0	0
3 M HNO_3	5	1	0	0.1

1161

1162

Table 2: Comparison of synthetic $CaCO_3$ treated with and without reductive cleaning reagent. Errors are 2x relative standard deviation (RSD) of secondary standards.

	Ca (wt %) ±10%	Mn /Ca (µmol/mol) ±4%	U/Ca (µmol/mol) ±8%	Mo/Ca (µmol/mol) ±12%
Uncleaned A	41.6	0.88	0.00117	0.70
Uncleaned B	39.3	0.88	0.00118	0.66
Cleaned A	34.9	0.60	0.00104	0.68
Cleaned B	33.9	0.58	0.00104	0.73

1163

Table 3: Concentration and isotope data for ODP758 unclean samples. ND = not determined.

Sample Name	Time (hrs)	Ca (wt.%)	Mn (ppm)	Sr (ppm)	Al (ppm)	Mn/Ca (µmol/mol)	Sr/Ca (µmol/mol)	Mn/Sr (ppm/ppm)	Al/Ca (µmol/mol)	Th/U (ppb/ppb)	U (ppb)	U/Ca (µmol/mol)	$\delta^{238}U$ (‰)	2SE (‰)	$\delta^{234}U$ (‰)	2SE (‰)	Mo (ppb)	Mo/Ca (µmol/mol)	$\delta^{98}Mo$ (‰)	2SE (‰)
ODP758 Unclean																				
0.2M acetic	24	19.4	58	718	32	218	1698	0.08	244	ND	71	0.061	-0.48	0.05	184	2	26	0.056	0.94	0.03
1M NaAC	24	25.1	101	913	138	295	1668	0.11	814	ND	77	0.070	-0.49	0.04	186	2	14	0.023	1.29	0.06
1M NH_4Ac	24	21.1	93	769	126	321	1675	0.12	888	ND	66	0.072	-0.54	0.03	182	2	7	0.014	1.09	0.06
1M acetic	24	19.9	119	707	427	435	1626	0.17	3176	ND	94	0.087	-0.53	0.03	164	2	5	0.012	0.24	0.09
0.2M HCl	1	18.7	103	699	407	402	1719	0.15	3233	ND	1	0.001	ND	ND	ND	2	2	0.005	0.74	0.2
0.5M HCl	1	21.1	245	787	1619	848	1709	0.31	11361	ND	111	0.110	-0.51	0.04	124	2	6	0.012	0.68	0.1
1M HCl	1	21.2	303	790	1702	1042	1707	0.38	11885	ND	100	0.112	-0.49	0.04	119	2	15	0.030	0.15	0.05
3M HCl	1	20.8	567	774	1937	1988	1707	0.73	13804	ND	88	0.125	-0.50	0.04	109	2	206	0.413	-0.45	0.02
7M HCl	1	21.4	626	795	2449	2128	1700	0.79	16926	ND	161	0.139	-0.43	0.05	104	2	312	0.607	-0.32	0.01
3M HNO_3	1	21.0	351	779	1986	1219	1698	0.45	13995	ND	111	0.122	-0.42	0.06	122	2	70	0.140	-0.1	0.02
0.2M HCl	24	16.7	61	692	13	265	1897	0.09	115	ND	55	0.076	-0.46	0.04	143	2	20	0.050	0.79	0.04
1M HCl	24	25.1	752	1643	3426	2190	3007	0.46	20264	ND	138	0.112	-0.49	0.04	116	2	73	0.122	0.05	0.02
3M HCl	24	21.9	660	1562	4627	2190	3258	0.42	31189	ND	155	0.132	-0.53	0.03	113	2	224	0.425	-0.13	0.02
Total Digest		25.6	886	1060	27716	2523	1898	0.84	160319	6.85	727	0.506	-0.37	0.04	-26	2	712	1.158	-0.29	0.02
7MHCl residue		0.3	70	52	21096	20353	36895	0.35	12375609	8.34	438	31.056	-0.35	0.04	-77	2	146	24.086	-0.6	0.03
1M NH_4Ac residue		0.3	613	50	22044	142772	27811	3.23	10432650	7.01	500	27.952	-0.36	0.04	-62	2	421	56.032	-0.19	0.03

Note: normalization to Ca uses Element XR data, except for Mo/Ca where isotope dilution is used.

Table 4: Concentration and isotope data for ODP758 samples that have undergone reductive cleaning. ND = not determined

Sample Name	Time (hrs)	Ca (wt.%)	Mn (ppm)	Sr (ppm)	Al (ppm)	Mn/Ca (µmol/mol)	Sr/Ca (µmol/mol)	Mn/Sr (ppm/ppm)	Al/Ca (µmol/mol)	U (ppb)	U/Ca (µmol/mol)	$\delta^{238}U$ (‰)	2SE (‰)	$\delta^{234}U$ (‰)	2SE (‰)	Mo (ppb)	Mo/Ca (µmol/mol)	$\delta^{98}Mo$ (‰)	2SE (‰)
ODP758 Clean																			
0.2M acetic	24	12.8	96	441	122	548	1579	0.22	1414	24	0.034	-0.53	0.06	177	2	1	0.005	ND	ND
1M NaAC	24	12.3	87	415	162	517	1543	0.21	1944	28	0.045	-0.63	0.09	182	2	2	0.008	ND	ND
1M NH_4Ac	24	11.6	87	374	145	548	1482	0.23	1854	31	0.052	-0.55	0.05	164	2	1	0.005	ND	ND
1M acetic	24	14.3	118	475	533	603	1521	0.25	5517	52	0.067	-0.53	0.04	125	2	1	0.004	ND	ND
0.2M HCl	1	12.7	105	414	1258	603	1494	0.25	14672	33	0.068	-0.49	0.04	97	2	1	0.005	ND	ND
0.5M HCl	1	12.7	106	423	1445	614	1534	0.25	16933	50	0.086	-0.55	0.04	103	2	9	0.030	1.35	0.07
1M HCl	1	12.2	104	409	1445	623	1538	0.25	17557	48	0.088	-0.55	0.05	103	2	5	0.019	2.11	0.1
3M HCl	1	12.4	108	420	1673	639	1557	0.26	20043	54	0.093	-0.48	0.05	133	2	13	0.045	0.86	0.05
7M HCl	1	10.9	109	363	1904	723	1520	0.30	25763	47	0.112	-0.55	0.05	131	2	122	0.770	0.07	0.02
3M HNO_3	1	11.9	107	412	1566	651	1581	0.26	19413	58	0.098	-0.54	0.05	107	2	7	0.025	ND	ND
0.2M HCl	24	14.8	149	533	1600	734	1651	0.28	16019	60	0.073	-0.51	0.04	103	2	0	0.001	ND	ND
1M HCl	24	13.8	143	573	2250	755	1900	0.25	24115	72	0.125	-0.57	0.04	102	2	10	0.030	1.04	0.07
3M HCl	24	13.6	165	492	3685	884	1656	0.34	40082	108	0.121	-0.63	0.08	106	2	38	0.119	0.82	0.04

Note: normalization to Ca uses Element XR data, except for Mo/Ca where isotope dilution is used.

1165

Table 5: Concentration and isotope data for mid-Cretaceous GA183 unclean samples. ND = not determined

Sample Name	Time (hrs)	Ca (wt.%)	Mn (ppm)	Sr (ppm)	Al (ppm)	Mn/Ca (µmol/mol)	Sr/Ca (µmol/mol)	Mn/Sr (ppm/ppm)	Al/Ca (µmol/mol)	Th/U (ppb/ppb)	U (ppb)	U/Ca (µmol/mol)	$\delta^{238}U$ (‰)	2SE (‰)	$\delta^{234}U$ (‰)	2SE (‰)

GA183 Unclean

0.2M acetic	24	21.5	236	626	23	800	1338	0.38	157	ND	30	0.035	-0.38	0.04	857	2
1M NaAC	24	27.3	286	921	51	764	1550	0.31	279	ND	57	0.039	-0.41	0.04	813	2
1M NH_4Ac	24	26.3	283	813	33	786	1419	0.35	184	ND	52	0.035	-0.33	0.03	833	2
1M acetic	24	30.5	333	963	104	794	1446	0.35	504	ND	61	0.037	-0.34	0.03	725	2
0.2M HCl	1	17.2	188	542	17	799	1448	0.35	145	ND	24	0.027	-0.18	0.05	647	2
0.5M HCl	1	29.3	314	949	311	782	1487	0.33	1574	ND	73	0.046	ND	ND	ND	ND
1M HCl	1	27.9	301	887	363	784	1455	0.34	1927	ND	67	0.046	-0.40	0.04	574	2
3M HCl	1	29.7	319	941	646	782	1453	0.34	3221	ND	68	0.049	-0.39	0.03	579	2
7M HCl	1	29.4	313	939	1410	776	1463	0.33	7100	ND	71	0.051	-0.36	0.03	619	2
3M HNO_3	1	30.3	319	952	541	768	1442	0.34	2647	ND	69	0.046	-0.35	0.03	562	2
Total Digest		31.1	370	975	19090	868	1441	0.38	91146	6.13	463	0.259	-0.39	0.04	-22	2
7MHCl residue		0.03	2	40	10113	5103	56164	0.06	45462376	3.20	230	114.661	-0.44	0.03	-164	2
1M NH_4Ac residue		19.5	28	255	9884	1041	5978	0.11	748744	5.65	284	1.821	-0.42	0.03	-122	2

1166

1167

Table 6: Concentration and isotope data for mid-Cretaceous GA183 samples that have undergone reductive cleaning. ND = not determined

Leachate acid	Time (hrs)	Ca (wt.%)	Mn (ppm)	Sr (ppm)	Al (ppm)	Mn/Ca (µmol/mol)	Sr/Ca (µmol/mol)	Mn/Sr (ppm/ppm)	Al/Ca (µmol/mol)	U (ppb)	U/Ca (µmol/mol)	$\delta^{238}U$ (‰)	2SE (‰)	$\delta^{234}U$ (‰)	2SE (‰)
GA183 Clean															
0.2M acetic	24	20.2	226	781	11	812	1770	0.29	79	29	0.045	-0.35	0.06	753	2
1M NaAC	24	19.7	208	600	19	769	1398	0.35	141	37	0.036	-0.39	0.04	702	2
1M NH_4Ac	24	19.3	219	584	13	825	1384	0.38	99	37	0.035	-0.27	0.04	701	2
1M acetic	24	21.3	229	659	46	782	1417	0.35	318	43	0.037	-0.34	0.04	655	2
0.2M HCl	1	15.9	177	522	188	805	1498	0.34	1741	13	0.048	-0.23	0.08	556	2
0.5M HCl	1	20.9	231	680	187	803	1491	0.34	1326	60	0.047	-0.33	0.04	518	2
1M HCl	1	18.3	202	594	214	805	1492	0.34	1741	41	0.048	-0.37	0.04	516	2
3M HCl	1	16.5	178	545	362	785	1510	0.33	3243	41	0.052	-0.34	0.04	512	2
7M HCl	1	18.6	208	613	920	817	1515	0.34	7347	46	0.054	-0.34	0.04	576	2
3M HNO_3	1	19.6	214	636	336	795	1488	0.34	2539	43	0.048	-0.34	0.04	499	2

1168

1169